ABSTRACT

Title of Document:	REEVALUATION OF ASCE 7-10 EXTERNAL PRESSURE COEFFICIENTS ON THE COMPONENTS AND CLADDING OF LOW-RISE BUILDINGS USING MODERN WIND TUNNEL TESTING DATA
	Matthew Lloyd Gierson, M.S., 2015
Directed By:	Assistant Professor, Brian M. Phillips (Chair) Professor, Bilal M. Ayyub, P.E. (Co-Chair) Dept. of Civil and Environmental Engineering

Wind loads for U.S. building designs are specified in a publication of the American Society of Civil Engineers (ASCE 7). Portions of the current version, ASCE 7-10, rely on wind tunnel tests that date back 30-50 years. In recent decades, advances in computer technology have allowed the simultaneous recording of many more pressure taps than was possible before. This research proposes a step-by-step methodology which determines the external pressure coefficients (GC_p) on the components and cladding of low-rise buildings using modern aerodynamic wind tunnel databases. Pressure tap time history data is used to calculate the peak pressure coefficients for a comprehensive sweep of arbitrarily selected grid areas, over all available tested wind directions. By incrementing grid area combinations with their contributing taps, GC_p can be plotted versus effective area. External pressure coefficients for the analysis of cladding and components are under predicted by the current ASCE 7-10 specifications.

REEVALUATION OF ASCE 7-10 EXTERNAL PRESSURE COEFFICIENTS ON THE COMPONENTS AND CLADDING OF LOW-RISE BUILDINGS USING MODERN WIND TUNNEL TESTING DATA

By

Matthew Lloyd Gierson

Thesis submitted to the Faculty of the Graduate School of the
University of Maryland, College Park, in partial fulfillment
of the requirements for the degree of
Master of Science
2015

Advisory Committee:
Professor Brian M. Phillips, Chair
Professor Bilal M. Ayyub, P.E., Co-Chair
Dr. Dat Duthinh, P.E.

Dedication

This thesis is dedicated to my family and loved ones
for their endless support and encouragement.

Acknowledgements

The work provided in this thesis was supported by the National Science Foundation's Louis Stokes Alliance for Minority Participation Bridge to the Doctorate (LSAMP-BD) Fellowship. Special thanks to Mrs. Taifa Simpson and the University of Maryland's Center for Minorities in Science and Engineering (CSME).

Research efforts were initiated thanks to the collaboration between Dr. Emil Simiu of the National Institute of Standards and Technology (NIST) and Prof. Bilal Ayyub of the University of Maryland. Dr. Dat Duthinh of NIST provided valuable guidance and a great deal of advice throughout the course of this research. Lastly, the efforts of Dr. Marc Levitan and Dr. Joseph Main of NIST have provided copious value in the production of this research.

Table of Contents

List of Tables

List of Figures

Chapter 1: Introduction

1.1. Motivation and Background

As hurricanes cause substantial damage to buildings, the accurate determination of wind pressures on a structure is key to the design of damage resistant components and cladding. Wind pressures specified for the enclosures of low-rise buildings in the current 2010 edition of the American Society of Civil Engineers 7 Standard (ASCE 7-10) are based on wind tunnel test data compiled 30 to 50 years ago. Significant upgrades in computing technology over the last half century have made it possible to perform wind tunnel tests that have higher levels of precision in recording pressure data. This precision is attributed to the wind tunnel facility's ability to collect time history data for many densely-distributed adjacent pressure taps at the same time. Incorporating the high frequency pressure wind tunnel testing method, these databases contain a comprehensive compilation of pressure affecting the external surfaces of a structure. Utilizing such modern aerodynamic pressure databases, this thesis discusses a methodology for analyzing such data and provides results for multiple buildings along with a partial comparison to the current ASCE 7-10 standard. The goal of this research is to develop a methodology which uses modern wind tunnel databases to reexamine the long-standing ASCE 7 standard for the external pressure coefficients affecting components and cladding.

Over the last twenty years, multiple wind tunnel databases have been created for low-rise buildings. Beginning in 2003, the University of Western Ontario (UWO), in cooperative agreement with the National Institute for Standards and Technology

(NIST) and Texas Tech University (TTU), released an aerodynamic database for low-rise buildings titled: Wind Tunnel Experiments on Generic Low Buildings. The objective of the UWO effort was to "conduct research to mitigate detrimental effects of wind storms on low-rise buildings and structures and on human activities" (Ho et al., 2003). Beginning in 2007, the Tokyo Polytechnic University (TPU) released an aerodynamic database for low-rise buildings titled: the TPU Aerodynamic Database for Low-Rise Buildings (Tamura, 2012). These two aerodynamic databases feature an assortment of tested building sizes, for which the building width, length, height, roof slope, and type of terrain vary. Both of these wind tunnel databases were compiled using the high frequency pressure testing method. Additionally, both of the databases are publically accessible, making them well-regarded tools in the wind engineering community.

In this thesis, a detailed literature review is first provided in Chapter 2 and contains: research that involves external pressure coefficients, a description of the low-rise building aerodynamic databases used in the analysis, and a review of multiple existing peak pressure estimating functions. Provided in Chapter 3 is the methodology developed for the analysis of wind tunnel tested low-rise buildings. The results of the applied methodology are presented, analyzed, discussed and compared with ASCE 7 standards in Chapter 4. The thesis concludes in Chapter 5 and explores intended future studies.

Chapter 2: Literature Review

2.1. Aerodynamic Databases for Low-Rise Buildings

2.1.1. Tokyo Polytechnic University's Wind Tunnel Database

Tokyo Polytechnic University's (TPU) aerodynamic database comprises a sizeable selection of wind tunnel tests that were performed to analyze wind loadings affecting both low-rise and high-rise buildings. TPU's aerodynamic database was developed as part of the Wind Effects on Buildings and Urban Environment, the 21st Century Center of Excellence Program, 2003-2007, and was funded by the Ministry of Education, Culture, Sports, Science and Technology, Japan. The objective behind the development of this database was to provide structural design engineers with wind tunnel test data regarding wind loads. TPU's aerodynamic database contains multiple sub-databases ranging from low-rise buildings with and without eave to high-rise buildings. Each of the distinct sub-databases, which can be found online via the TPU aerodynamic database website (Tamura, 2012), are listed as follows: Wind Pressure Database for High-Rise Building, Wind Pressure Database of Two Adjacent Tall Buildings, Database of Isolated Low-Rise Building Without Eaves, Database of Isolated Low-Rise Building With Eaves, and Database of Non-Isolated Low-Rise Building. The majority of this study solely focuses on the sub-database of isolated low-rise buildings without eave from TPU.

The sub-database, isolated low-rise buildings without eave, contains variables categorized in the following order: roof type, height to breadth ratio, depth to breadth ratio, and roof pitch. Figure 2.1 provides example dimensions of breadth *B*, depth *D*,

eave height *H0*, roof pitch β, and wind angle θ of a typical building. This particular database contains a wide variety of tested buildings, including three roof types, various building geometries and multiple combinations in which the roof slopes were varied. Each of the building combinations contains corresponding data files which were developed using the following wind angles θ: 0, 15, 30, 45, 60, 75, and 90 degrees. TPU's decision to limit tests up to 90 degrees comes from the large expense required for performing each wind tunnel test and therefore accommodates the wide variety of tested building geometries. Additionally, the rectangular building dimensions allow for a mirror of the worst case minimum and maximum envelope pressures to each of the four identical portions of the structure. Thus, the researchers felt it best to reduce the required amount of testing data for analysis and evaluation by limiting the wind angles tested.

TPU's database is publically available for download as MATLAB files (Tamura, 2012). The database files contain the buildings geometric information including: eave height, breadth, depth, and roof slope. Each of the associated pressure taps is provided an identification number, a surface number, and its *x* and *y* coordinates.

Table 2.1: TPU's tested low-rise buildings without eave case numbers and building attributes (Tamura, 2012)

Case Number	Roof Type	Breadth B (m)	Depth D (m)	Eave height H0 (m)	Roof pitch β (degrees)
1-12	Flat	16	16, 24, 40	4, 8, 12, 16	0
13-44	Gable	16	16	4, 8, 12, 16	4.8, 9.4, 14, 18.4, 21.8, 26.7, 30, 45
45-76	Gable	16	24	4, 8, 12, 16	4.8, 9.4, 14, 18.4, 21.8, 26.7, 30, 45
77-108	Gable	16	40	4, 8, 12, 16	4.8, 9.4, 14, 18.4, 21.8, 26.7, 30, 45
109-116	Hip	16	24	4, 8, 12, 16	26.7, 45

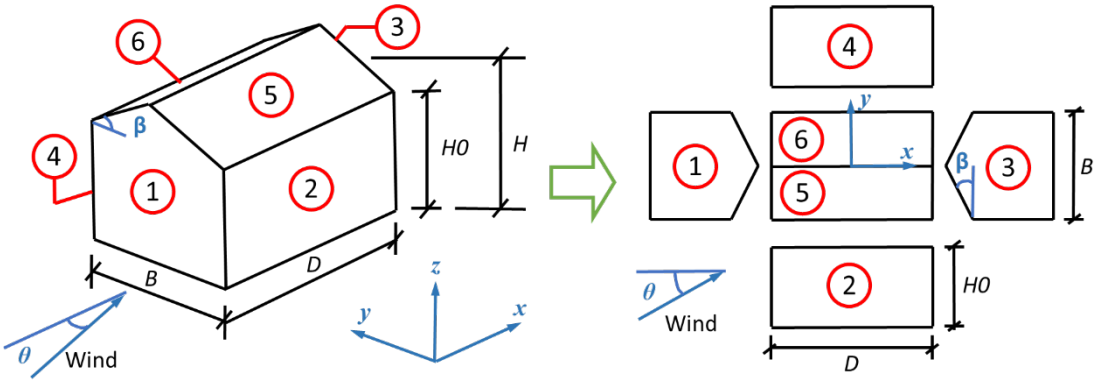

Figure 2.1: TPU test model and definitions of geometrical parameters and coordinates (Tamura, 2012)

TPU's Boundary Layer Wind Tunnel is 2.2 m wide by 1.8 m tall. The wind tunnel tests were performed at the following scales: a geometric (length) scale of 1/100, a velocity scale of 1/3, and a time scale of 3/100. Tests were performed in accordance to terrain category III (suburban) as defined in the Architecture Institute of Japan (AIJ, 2004). According to Tamura (2012), the turbulence density at a height of 10 cm was roughly 0.25. Additionally, the test wind velocity at a height of 10 cm was roughly 7.4 m/s, which corresponded to 22 m/s at a height of 10 m in full scale. This wind speed corresponds to the mean hourly wind speed as utilized in ASCE 7-10 calculations. Wind pressure coefficient time-history data, sampled at 500 Hz, are provided in TPU's database files. The datasets correspond to roughly 10 minutes of full scale data, or 18 seconds of model scale data.

TPU's aerodynamic database incorporates a moving average calculation as shown by Eq. (2.1) to the time series data provided in the database. The purpose behind incorporating the moving average to the time series data was to smooth out the observed rough peak values, which can be unnatural when scaling the model to full scale. In Eq. (2.1), Δt represents the duration of the wind pressure coefficients, $C_{p\_ori}(i,t)$

is the original wind pressure coefficient data for each measured pressure tap *i* at time *t*. This moving average was calculated every 0.006 s in model scale and corresponds to 0.2 s in full scale.

$$C_p(i,t) = avg(C_{p_{ori}}(i,t-\Delta t), C_{p_{ori}}(i,t), C_{p_{ori}}(i,t+\Delta t)) \quad (2.1)$$

The following calculations outline the method which TPU used for calculating the normalized wind pressure coefficients $C_p(i,t)$, from each individual taps measured wind pressure data p_i. The calculation for $p(i,t)$ of Eq. (2.2) represents the net tap pressure above ambient/reference pressure and is expressed by subtracting the individual tap measured wind pressure data p_i by the static atmospheric pressure p_0 at the reference height, which is defined by Tamura (2012) as the mean roof height *H*.

$$p(i,t) = p_i - p_0 \quad (2.2)$$

The value p_H of Eq. (2.3) represents the reference wind pressure of the approaching wind velocity at the mean roof height and is calculated using the mean hourly wind speed V_{3600} at reference height and the air density ρ.

$$p_H = 0.5\rho V_{3600}^2 \quad (2.3)$$

The normalized wind pressure coefficients are denoted by $C_p(i,t)$ at tap *i* and time *t* and are calculated by dividing the net tap pressure by the reference wind pressure as in Eq. (2.4). To make the wind pressure coefficients correspond to a full scale duration of 0.2 s, TPU uses a moving average over 0.006 s of the measured time series (Tamura, 2012).

$$C_p(i,t) = p(i,t)/p_H \quad (2.4)$$

2.1.2. University of Western Ontario's Wind Tunnel Database

The University of Western Ontario's (UWO) aerodynamic database comprises of a variety of tested low-rise buildings that incorporate a high density of pressure taps located in particular regions of high pressure gradients. The UWO wind tunnel database was developed to analyze the wind load acting on low-rise buildings and is part of the NIST/TTU Cooperative Agreement – Windstorm Mitigation Initiative.

The first phase of UWO's experimental program developed by Ho et al. (2003) tested a variety of geometric plan dimensions, while varying the eave heights and respective roof slope angles. Five variations of low-rise building plan geometries were tested, and are listed in Table 2.2. All of the buildings tested for phase 1 were gable shaped buildings. Each of the building combinations contains corresponding data files which are available for a wide variety of wind angles θ ranging in increments of 5 degrees between 0 to 90 degrees and 270 to 360 degrees. The omission of tests greater than 90 and less than 270 degrees was applied in consideration of the large expense for running each wind tunnel test. Similar to TPU, the rectangular building dimensions allow for a mirror of the worst case minimum and maximum envelope pressures to the other portions of the structure.

Table 2.2: UWO's database of low-rise buildings (Phase 1) tested building attributes

Test number	Roof type	Breadth B (ft)	Depth D (ft)	Eave height H0 (ft)	Roof pitch β (degrees)
1	Gable	80	125	16, 24, 32, 40	4.76
2	Gable	80	125	16, 24, 32, 40	14
3	Gable	80	125	16, 24, 32, 40	1.19
4	Gable	40	62.5	12, 18, 24, 40	4.76
5	Gable	160	250	12, 18, 24, 40	4.76

UWO's Boundary Layer Wind Tunnel was used for the models listed in Table 2.2, and is 3.4 m wide by 1.8 to 2.7 m high. The wind tunnel tests were performed at the following scales: a geometric (length) scale of 1/100, a velocity scale of 1/3.2 and a time scale of 3/100. Tests were performed for two different exposure categories, open country and suburban, which are in accordance to the exposure types conforming to ASCE 7-10. According to UWO, the turbulence density at a height of 10 cm was roughly 0.19. The wind speeds recorded correspond to mean hourly wind speeds as utilized in ASCE 7-10 calculations. Wind pressure coefficient time-history data, sampled at 500 Hz, is provided in UWO's database files. The datasets correspond to approximately 60 minutes of full-scale data, or 100 seconds of model scale. The time history pressure values provided in UWO's database do not incorporate a moving average, unlike TPU's database.

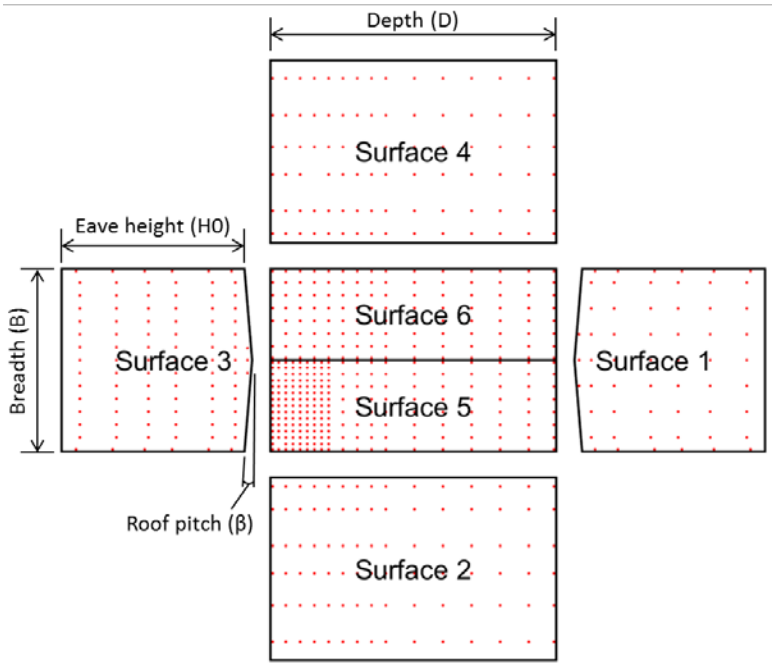

Figure 2.2: UWO flattened test model with definitions of geometrical parameters

Each of UWO's database files provide the buildings geometric parameters as length, width, and eave height. In order to compare these dimensions to TPU, these parameters were renamed to become breadth (previously width) and depth (previously length) while eave height remained consistent. A flattened view of a building tested in UWO is provided in Figure 2.2. Additionally, Figure 2.2 provides UWO's defined surface numbers, and appropriate geometrical parameters. Figure 2.2 also contains red dots which resemble the pressure taps plotted in their respective locations along the flattened surfaces of the building.

2.2. Comparison of TPU's and UWO's Wind Tunnel Databases

Previous research conducted at Florida International University (FIU) compared three geometrically similar buildings from the TPU aerodynamic database to the UWO aerodynamic database (Hagos et al., 2014). For each surface, Hagos et al. (2014) typically selected three to five neighboring pressure taps, which shared similar locations between the databases. For three different wind directions (0, 45, and 90 degrees) they estimated the peak pressure coefficients, using the method developed by Sadek and Simiu (2002). The researchers concluded that the peak results from the examined pressure taps show minor differences between the two databases, and are therefore regarded as equally valid. It is important to note that there are differences between the databases in building sizes, tap resolution, etc., meaning that the databases are not redundant, simply that they are comparable in overlapping scenarios.

Researchers Habte, F., Chowdhury, G., and Simiu, E., are leading a study out of FIU to quantify the effects of reducing aerodynamic time history data on wind load

calculations (Duthinh et al., 2015). The purpose for this study is to reduce the large volume of data that accompanies wind tunnel test databases, without compromising the validity of the data. The three minor time series transformation efforts tested to reduce the volume of this data were: (i) record length reduction, (ii) sampling rate reduction, and (iii) data compression by wavelet techniques. In addition to these methods for volume reduction, the application of a time averaging technique, also used in TPU's database, was implemented and analyzed. The study explains that TPU's incorporation of the moving average aids in eliminating artificially high peaks, which are inherent for eddy sizes too small to have an effect, from a structural point of view. After separately analyzing each of the three transformations and comparing the results to initial pressure coefficients, the ratios were only marginally higher for each transformation, typically by only 1-2%. Based on these minimal percent differences, the study concludes that applying these minor time series transformations is acceptable for reducing the volume of data required for other aerodynamic data analysis purposes. As demonstrated in the study, the moving average calculation incorporated by TPU has little affect on the time series data, and direct comparison of the TPU data (with time averaging) with the UWO data (without time averaging) is justified.

2.3. Peak Pressure Estimation Methods

Wind tunnel tests are scaled down in both length and time when compared to their full-scale analogs. In particular, the fluctuations in wind pressure are only explicitly known for the model's scaled duration of the test. Analysis of wind tunnel time history data relies on algorithms for finding the peak pressures over a standard

duration of time. These peak pressure estimation methods must consider the random nature of the wind in order to properly evaluate the peak values; it should be noted that a repeat of a wind tunnel test, or a test of longer duration, would yield different peak pressure values as a result of the wind's innate randomness. Analysis of time series pressure data often requires the adjustment of the full scale duration of the test extended to a 60 minute wind storm; this scaling is required for comparison with the ASCE 7-10 standards. Multiple methods for obtaining the expected peak pressures are available such as the zero upcrossing method developed by Rice (1944) and the Best Linear Unbiased Estimator (BLUE) developed by Lieblein (1974).

A demonstration of the pressure time history data obtained from a TPU wind tunnel test is provided below to aid in the understanding of the peak estimation procedure. Figure 2.3 shows the location of two selected pressure taps, tap 85 and tap 114, which will be used for comparison in this example, on the surface of a studied gable building named TPU-1 and presented further in Chapter 4.1. In this example, tap 114 is located on the windward wall and tap 85 is located close to the windward external edge of the roof. Note, the other taps located over the building were ignored for the sake of this example. Additionally, it should be pointed out that the data shown in Figure 2.4 is normalized with respect to the hourly wind speed, whereas later results are normalized with respect to the three second gust speed. In Figure 2.4, the two tap's pressure coefficient time history data were plotted concurrently, for a wind direction of θ equal to 0 degrees. The variations of the recorded pressure data can be observed as tap 85 exerts strictly negative suction pressure and tap 114 contains only applied

positive pressure. It is therefore obvious that the pressure can significantly vary as a function of the tap's location on the building's surfaces.

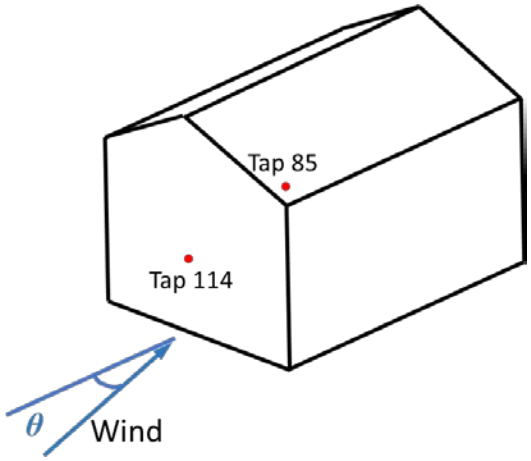

Figure 2.3: Location of two selected pressure taps for pressure coefficient comparison

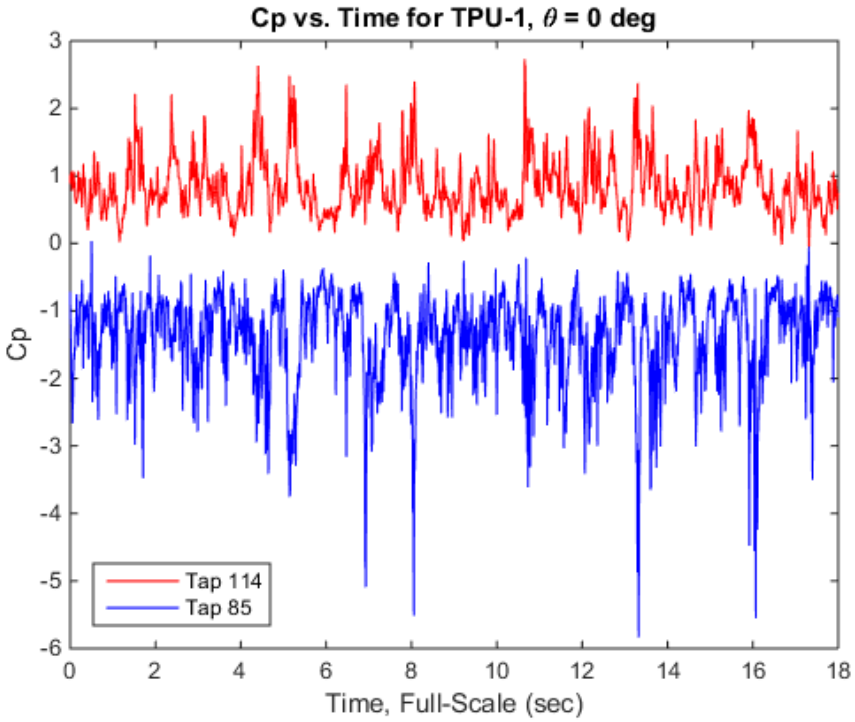

Figure 2.4: Plot of Cp vs. Time for pressure tap 85 and 114 from TPU-1

A histogram of the time series pressure data for both taps is presented in Figure 2.5. As previously mentioned, the variation between each pressure tap is attributed to

the difference in pressure as a function of the tap's location on the surface of the building. Interpreting the histogram of pressure tap 85, it can be observed that the behavior of the tail of the minimum values is significantly different than the tail of the maximum values; this can also be observed in the tails of pressure tap 114. As the tails of the distribution vary for each pressure tap, it is important to implement a peak estimation method which considers this variation and provides the highest level of accuracy when estimating the values in the tails of the distribution.

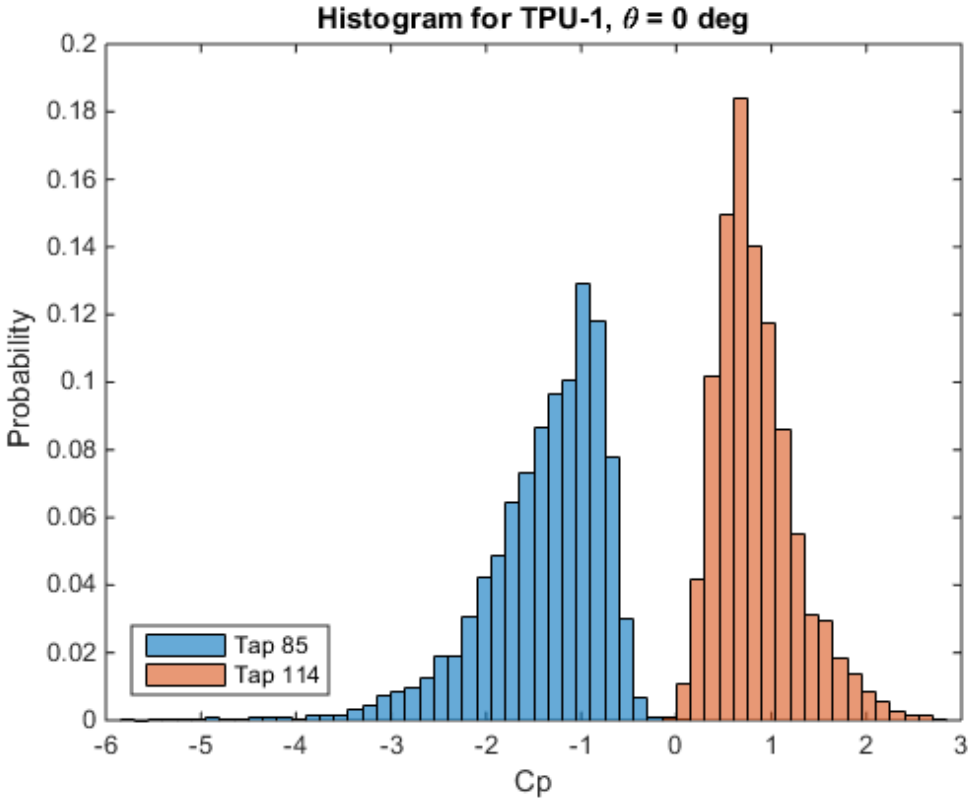

Figure 2.5: Histogram of pressure tap 85 and 114 from TPU-1

Early attempts for obtaining the peak values from time series data dealt only with considering the observed peaks and/or fitting statistical curves to several observed peaks (Peng et al., 2013). These attempts eventually evolved towards the estimation of

such peaks by fitting the Extreme Value Type 1 (Gumbel Distribution) to the observed peaks over a certain duration, and then extending this duration as needed.

Sadek and Simiu (2002) further modified Rice's zero upcrossing method (1944) in order to apply the peak estimating method to non-Gaussian processes. Sadek and Simiu concluded via statistical testing that, for the purpose of estimating peaks, gamma and normal distributions could appropriately model the marginal distribution fitting with regards to the time series' histogram's longer and shorter tails, respectively. As a result of the study, it was found that the distribution of the peaks can be represented by the Extreme Value Type I (Gumbel) distribution. Main (2011) programmed this peak estimation method into a MATLAB function, titled Maxminest, which returns the expected maximum and minimum values of the input time series. The function Maxminest is publically available on the NIST Statistical Engineering Division (2004) website.

A second procedure, developed by Lieblein (1974), is known as the Best Linear Unbiased Estimator (BLUE) and also considers the data as non-Gaussian and provides a different method for determining the peaks. The BLUE method involves separating the time series data into epochs and then fitting a Gumbel distribution to the observed maxima values from each of those epochs. The BLUE method has been widely used for peak estimation processes, but was not applied for the study presented in this thesis.

MATLAB (2014) provides multiple functions which can be utilized for curve fittings of the Generalized Extreme Value (GEV) distributions. These available functions account for the three cases of extreme value distributions, which are titled Gumbel, Frechet, and Weibull and are often referred to respectively as Types I, II and

III. Application of MATLAB's GEV functions provides the shape, scale and location parameters from the inputted data points. Selecting the input data as observed maxima for arbitrarily selected epochs allows the GEV functions to provide the maximum likelihood parameter estimates of the GEV, which can be inverted to obtain the expected peak values for a given probability of exceedance.

Particular studies have been made to observe the behavior of the proposed non-Gaussian peak estimators. Peng et. al. (2013) determined that the non-Gaussian peak estimators perform well for mildly non-Gaussian data, but poorly for strongly non-Gaussian data. Their study also provides an alternative method for analysis of the strongly non-Gaussian data, called the Hermite polynomial model (HEM); the study suggests that the HEM method provides more accurate and less biased results when analyzing the non-Gaussian data.

The procedure used herein for peak pressure estimations is based on Rice's zero upcrossing method, modified by Sadek and Simiu (2002) to apply to non-Gaussian processes, and programmed by Main (2011) into a MATLAB function. The method notes that the peak pressures are generally non-Gaussian and can be represented by the Extreme Value I (Gumbel) distribution.

Chapter 3: Methodology for Computing Peak Envelope External Pressure Coefficients

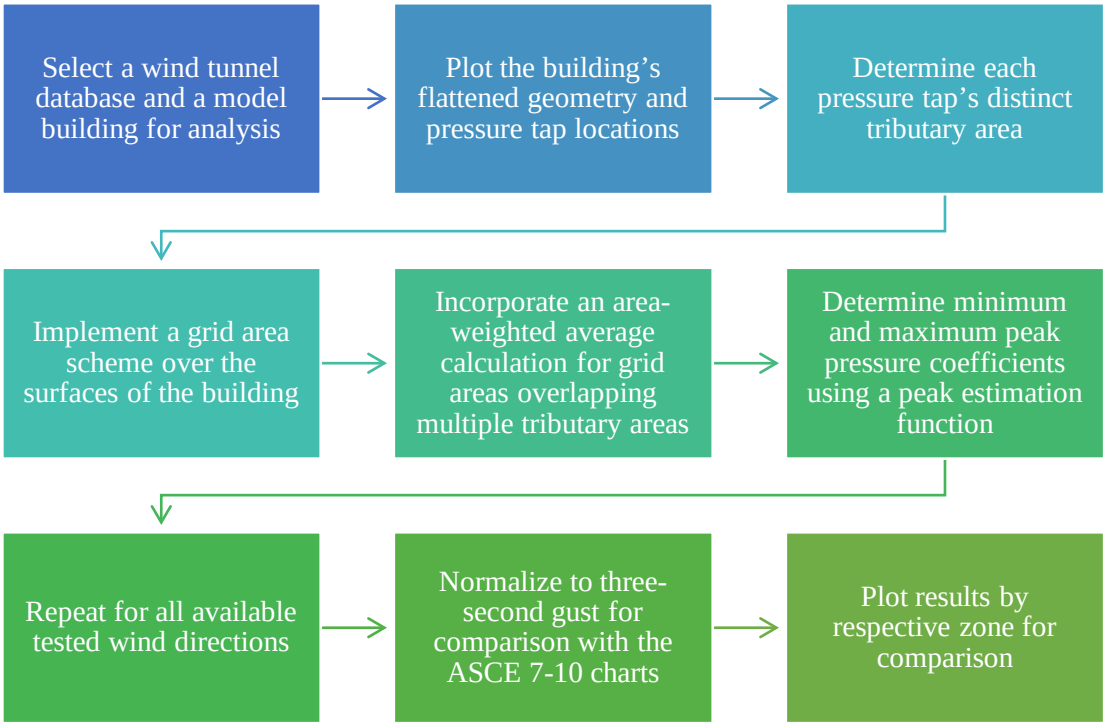

Figure 3.1: Methodology simplified step by step

The methodology used to analyze the wind velocity pressure coefficients of low-rise buildings is summarized in Figure 3.1, and is explained in detail as follows. The method begins by selecting a wind tunnel database and a building for analysis. A typical database file contains the location of each pressure tap along with its respective pressure time history data for the tested wind directions. Other related attributes are also provided, such as the terrain exposure, wind speed, model scale and building dimensions and roof style. It should be noted that the methodology can be applied to any low-rise building roof style from TPU or UWO's database, including flat, gable and hip roofs with only minor modifications.

In order to observe the building's geometry and tap distribution, the building is first flattened and plotted displaying the location of each of the pressure taps and outlining the boundaries of the building's surfaces. This plot provides the grounds for which the tap tributary areas can be determined.

The method adopted to obtain distinct tributary areas for assigning the pressure coefficient time history data to the irregularly spaced pressure taps is called the Voronoi diagram (Voronoi 1908, MATLAB 2014). In order to effectively assign the pressure coefficient time history data to the surfaces of the building, each pressure tap's tributary area must first be explicitly defined. The Voronoi diagram function provided in MATLAB can be used to account for these potential irregular tap distributions, by determining the confining area closest to each pressure tap and defining it as a polygon or as the tributary area for this study. However, as the Voronoi diagram function provided in MATLAB does not provide the option of specifying a boundary, the exterior points then have areas which extend to infinity. Therefore, as boundaries were required to confine the surfaces of the building, a separate function was employed named VoronoiLimit by Sievers (2015) which allowed for the determination of the tributary areas inside a bounded domain.

The Voronoi diagram builds upon a Delaunay triangulation (Delaunay 1934, MATLAB 2014) which begins with a set of points/tap locations that are connected forming triangles that: (1) do not overlap, (2) cover the entire interior space formed by the points, and (3) do not have any points within the triangle's circumcircle. Next, a Voronoi diagram is created by drawing straight lines perpendicular to the triangle boundaries, equidistant from the boundaries' vertices. Regions are formed from these

lines that encompass one point each, with every location in the region closer to that point than to any other point.

In order to demonstrate the application of the Voronoi diagram to irregularly spaced pressure taps, four images were assembled and shown in Figure 3.2. Figure 3.2 shows elevation views for the wall of a gable building with a roof slope of 45 degrees from TPU's database. Pressure tap locations are marked by red circles and tap tributary area boundaries are marked by blue lines (between vertices) and by blue circles (at the vertices). Note, for all of the Voronoi diagram figures provided in this study, there is no significance between the size of the red circles and the size of the corresponding pressure tap. Figure 3.2(a) provides the location of the individual pressure taps with no tributary areas defined. Figure 3.2(b) shows an example in which 2 m × 2 m tributary areas were assigned to each pressure tap, on center. Figure 3.2(c) provides an example where the Delaunay triangulation was applied. This method was not directly useful for defining tributary areas about each pressure tap as it uses the locations of each pressure tap for the triangulation corner connections. Additionally, the Delaunay triangulation was bounded by the inputted pressure tap coordinates and not by the surface of the building. Figure 3.2(d) provides an example of the applied Voronoi diagram; it can be observed that this method provides an automated technique to determine the tributary areas for irregularly spaced pressure taps.

The Delaunay triangulation faced problems when attempting to consider the edge surfaces of the building, as a provided surface coordinate would be considered similar to a pressure tap location; therefore, the taps closest to the buildings edge surface would connect directly to the corners of the building, and would ignore the edge

surfaces between these corners of the building. On the other hand, the Voronoi diagram was able to consider the bounded region of the edges of the building and proceed with identifying each tap's tributary areas. To observe the cooperation between the Delaunay triangulation and the Voronoi diagram, each of these methods was superimposed on Figure 3.3, where the red dots represent the pressure taps, red lines represent the Delaunay triangulation, and blue lines represent the Voronoi diagram's tributary area boundaries. Demonstrations of the Voronoi diagram applied to one building from each of the two databases (TPU and UWO), are provided respectively in Figure 3.4 and Figure 3.5. Subsequently, Figure 3.6 provides an enlarged perspective of the highly populated pressure tap region from a building in UWO's database to appropriately show the Voronoi diagram's efficiency in handling highly populated tap regions.

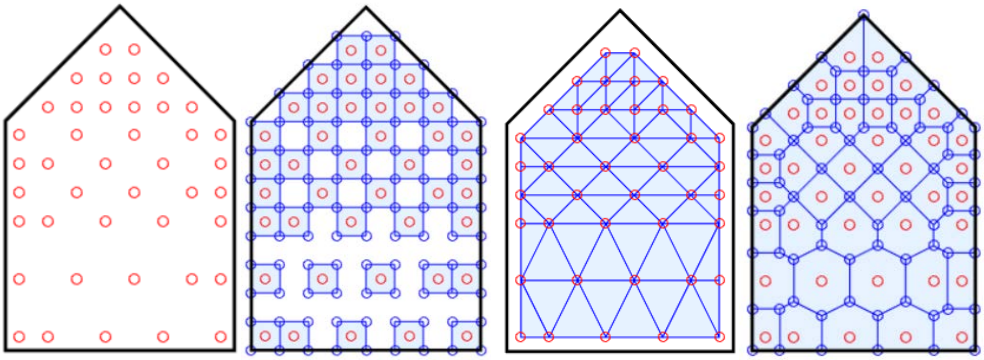

Figure 3.2: Examples of pressure tap tributary areas

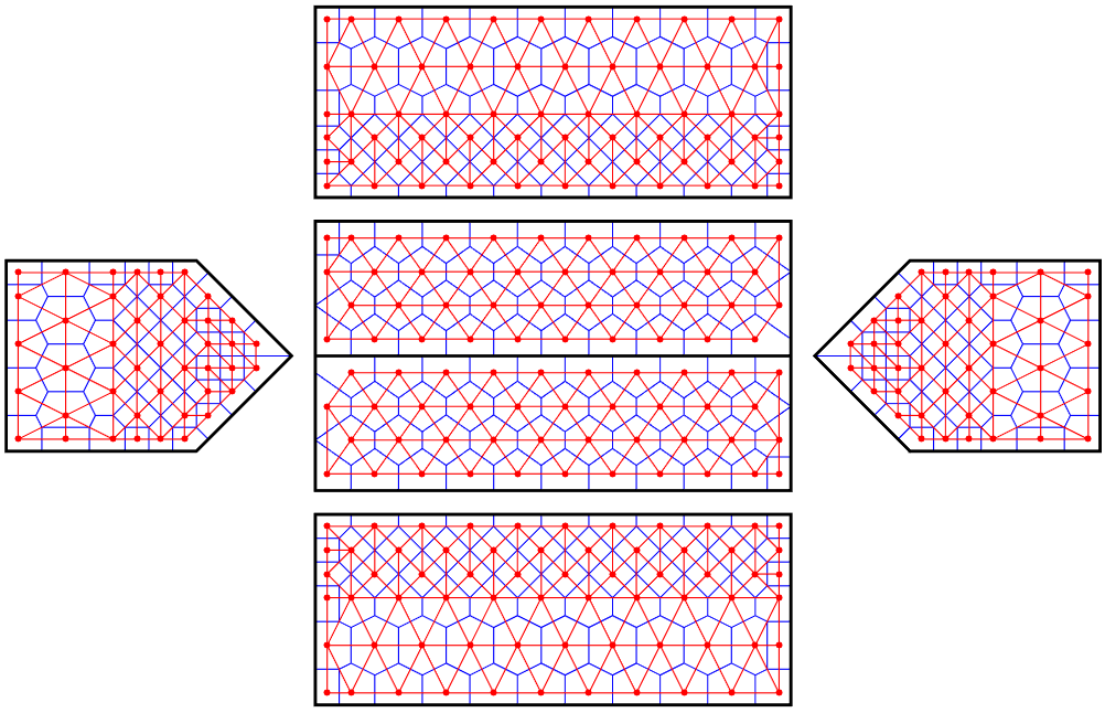

Figure 3.3: Voronoi diagram superimposed over the Delaunay triangulation

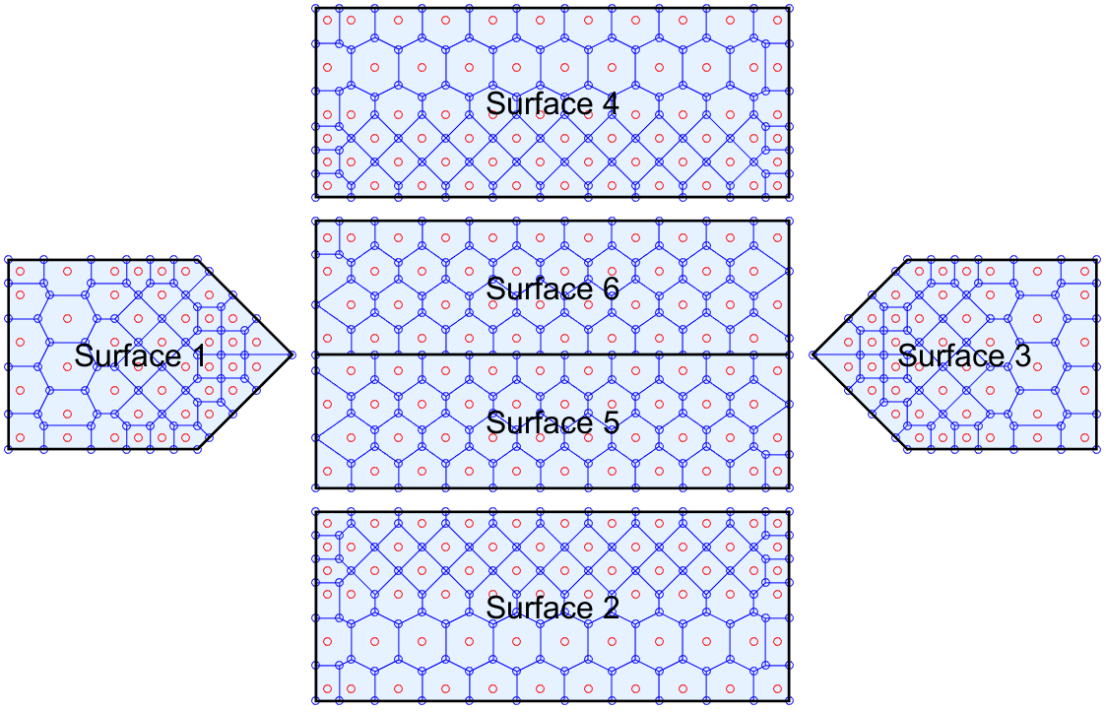

Figure 3.4: Voronoi diagram applied to a gable building (β=45 degrees) from TPU's database

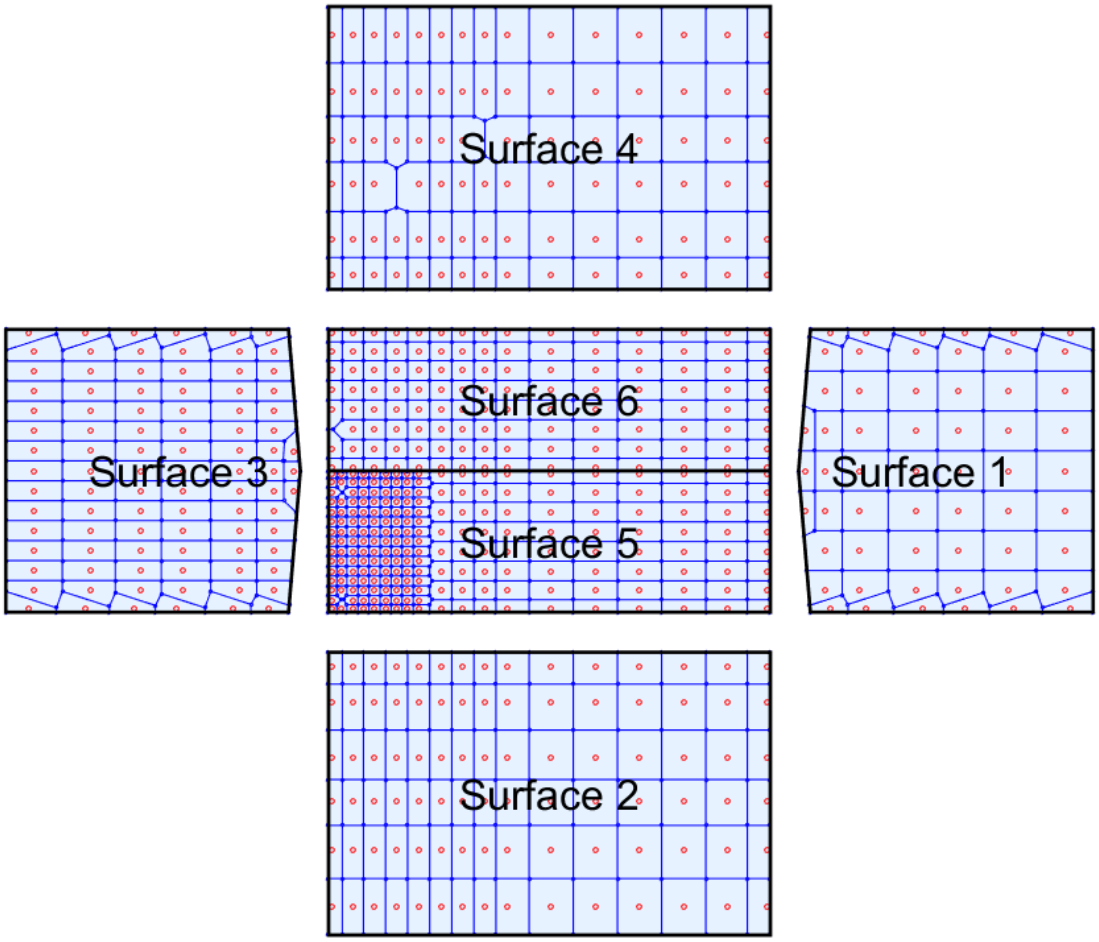

Figure 3.5: Voronoi diagram applied to a gable building (β=4.76 degrees) from UWO's database

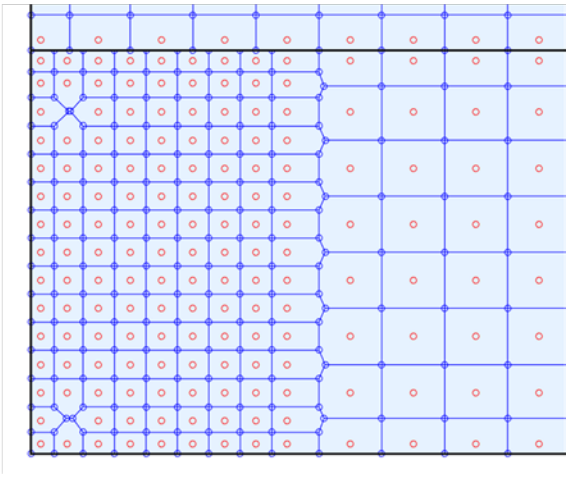

Figure 3.6: Enlarged view of the highly populated pressure tap region from Figure 3.5 Surface 5 (surface number not displayed in figure)

Next, grid areas were implemented in the methodology to calculate the wind pressure coefficients varying as a function of area and location. In order to evaluate ASCE's external pressure coefficient charts, the size of the grid areas and the offset dimensions of the grid need to be incremented. The grid areas are laid out starting at a selected corner of each surface and are then propagated from the corner until the grid best covers the surface's area. As the grid areas occasionally cross outside of the building surface boundary, it was chosen to discard the data for these partial grid areas in order to keep the results consistent with the chosen grid area combinations, which are described below.

The minimum grid area dimension is determined based on the smallest absolute distance between individual taps. This decision was made as there is no justification to resolve a smaller grid area than the smallest tributary area. For instance, for the TPU low-rise building without eave database, the smallest absolute distance between pressure taps is 2 m, which resolves the smallest grid area as 2 m × 2 m. The largest grid size was selected based on judgement. In this analysis, the largest aspect ratio for the grid area dimensions was set to 3.5.

An offset of the grid area is incorporated to shift the grid area, acquiring the worst case pressure coefficient value which is a function of each grid area's location. The grid area offset begins with zero offset, and then adds a selected offset value to the y-direction. This addition is repeated until the y-offset value reaches the grid area y-dimension, then the grid area x-offset value is incremented once and the y-offset value is reset. This process is repeated until the x-offset and y-offset have both reached the current grid area dimension. After which, the grid area dimension is then incremented

and the process is repeated for all grid area combinations and their offsets. Figure 3.7 provides examples of the method of superposing and offsetting grid areas over one wall of a gable building, where the smallest and largest grid areas were selected as 2 m × 2 m and 3 m × 3 m respectively, with an increment of 1 m. Additionally, the grid area offset increment was selected as 1 m. Figure 3.7 (a) shows a superposed 2 m × 2 m grid area with no offset. Figure 3.7 (b) shows the same 2 m × 2 m grid area with 1 m offset in each direction. Figure 3.7 (c) shows a 2 m × 4 m grid area with no offset. Figure 3.7 (d) shows a 2 m × 4 m grid area with 1 m offset in the x-direction. Note, Figure 3.7's color scale is related to Figure 4.18, but is unimportant here other than to mean that the grid areas with filled color contain pressure data, where those that do not are white. It should be noted that results presented throughout this study do not show the grid areas that fall outside of the building's surface as white, as is done in Figure 3.6; however, these specific grid areas were discarded before the pressure coefficient results were collected and plotted by zone.

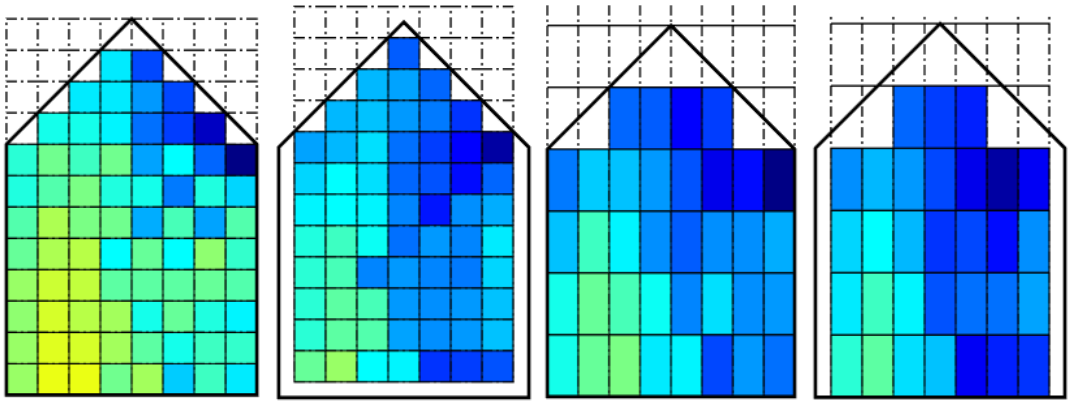

Figure 3.7: Example of grid area sizes, incremens and offsets

An example is provided below to show all possible grid area combinations and their respective offsets for a limited case of grid area sizes. In this example, a minimum

grid size of 2 m × 2 m is selected and then incremented by 1 m in each direction to achieve grid sizes up to a maximum of 3 m × 3 m. Additionally, these grid areas are offset in each direction by a specified increment, say, 1 m. The possible grid area/offset combinations are then shown in Table 3.1, and the number of grid area combinations for this example totals to 25.

Table 3.1: Example provided for grid area combinations

x (m)	2	2	2	2	2	2	2	2	2	2	3	3	3	3	3	3	3	3	3	3	3	3	3	3
y (m)	2	2	2	2	3	3	3	3	3	3	2	2	2	2	2	2	3	3	3	3	3	3	3	3
x offset (m)	0	0	1	1	0	0	0	1	1	1	0	0	1	1	2	2	0	0	0	1	1	1	2	2	2
y offset (m)	0	1	0	1	0	1	2	0	1	2	0	1	0	1	0	1	0	1	2	0	1	2	0	1	2

In order to find the pressure coefficient time history of any selected grid area, an area-weighted average calculation must be performed. The area-weighted average calculation uses the surrounding pressure tap's tributary areas, however, only where the pressure tap's tributary area's overlap with the selected grid area, to apply each of the tap's pressure coefficient time history results to the grid area. For instance, when a grid area overlaps with the tributary area of only one pressure tap, then the grid area's pressure coefficient time history will remain the same as that of the individual tap. However, when a grid area contains more than one pressure tap's tributary areas, then an area-weighted average calculation of the time histories of those tributary areas which overlap with the grid area must be performed to determine the grid area's pressure coefficient time history.

Hourly wind pressure coefficients GC_{p3600} are determined by an area-weighted average calculation in which the tributary areas a_i of all taps i which fall into the grid area of interest are multiplied by their respective wind pressure coefficients $C_p(i,t)$ and then the sum is divided by the grid area of interest A; this process is summarized by Eq.

(3.1). Also, the sum of the overlapping tributary areas is equal to the grid area, as demonstrated in Eq. (3.2). In Eq. (3.1), the peak factor *G* accounts for variability of the pressure coefficient due to the randomness of the aerodynamic response and is introduced implicitly when the averaging process and the peak selection process are applied (Simiu, 2011).

$$GC_{p3600} = \frac{\sum a_i \, C_p(i,t)}{A} \tag{3.1}$$

$$A = \sum a_i \tag{3.2}$$

Peak pressure coefficient values are obtained in each grid area using the Rice method (Sadek and Simiu, 2002), which consists first in estimating the mean upcrossing rate of a given threshold from the spectral density function of a random process. From this estimate, the cumulative distribution function of the largest peaks is calculated for a given time interval. The calculation of distributions of non-Gaussian peaks is based on a standard translation process, which requires fitting an optimal marginal distribution to the shorter tail and another to the longer tail of the time series of interest's histogram. For the histogram's longer tail, the three-parameter Gamma distribution is fitted for the purpose of peak estimations. For the histogram's shorter tail, a normal distribution is used for the purpose of peak estimations. The extreme values of both tails can be simultaneously represented by a parent distribution, corresponding to the Extreme Value Type I (EVI) Gumbel distribution (Sadek et. al., 2002).

This method of calculating the peaks was implemented by Main (2011) in a MATLAB function Maxminest and is publically available on the NIST Statistical Engineering Division (2004) website. Inputting the pressure coefficient time history

data of any pressure tap along with a duration ratio to the Maxminest function, provides an output of the maximum and minimum peak pressure coefficient mean values. In the case of obtaining the peak pressure coefficients, the mean value is obtained from Extreme Value Type I (Gumbel) distribution. Demonstrated in Eq. (3.3), is the equation for calculating the duration ratio parameter D_R to account for the fact that the expected peak pressures in a 60-minute storm are different from the peaks derived from a 10-minute (full scale) wind tunnel test record.

$$D_R = \frac{\text{duration of storm of interest}}{\text{full-scale duration of measured record}} \tag{3.3}$$

The calculation of the peak pressure coefficients is repeated for each grid area over all of the available tested wind directions. The worst case result is selected from each grid area across all of these wind directions to populate the values into an enveloping plot. This procedure is demonstrated in the results section for all available wind directions of a selected building from TPU's database.

To compare the calculated minimum and maximum peak wind pressure coefficients to the ASCE 7-10 values, the hourly wind speed must be renormalized to a peak three-second gust. The three-second gust speed V_3 can be taken as 1.52 times the hourly wind speed V_{3600} (Durst, 1960). This factor is demonstrated by performing the following calculations, where the wind pressure coefficient for the three-second gust is represented by GC_{p3} and the 3600 s storm wind pressure coefficient is represented by GC_{p3600}. ASCE 7-10 external peak pressure coefficients are simply identified as GC_p, corresponding to GC_{p3} in Eq. (3.4).

$$GC_p = GC_{p3} = GC_{p3600}\left(\frac{V_{3600}}{V_3}\right)^2 = GC_{p3600}\left(\frac{1}{1.52}\right)^2 \tag{3.4}$$

Results using the proposed method are then compared to ASCE 7-10 external pressure coefficient charts by applying the zoning specifications. External pressure coefficients are specified by particular figures in the ASCE 7-10 specifications. Each figure contains a chart which provides the recommended external pressure coefficient value corresponding to effective wind area and respective zone. The particular zones are defined over the surfaces of the building and separate the walls or roofs by zones of significantly differing pressures. The determination of zones varies by building roof type and roof pitch. The zones and external pressure coefficients are provided for enclosed and partially enclosed buildings for walls in Figure 30.4-1, and for gable/hip/flat roofs in Figures 30.4-2A, -2B, -2C (ASCE 7-10). Each of these figures contains unique attributes and guidelines for determining the zones on the wall and roof surfaces of the building and for determining the external pressure coefficient value. For example, the external pressure coefficients of walls should be reduced by 10%, when the building's roof slope is less than or equal to 10º. Specific explanations are provided in the next two paragraphs for obtaining the zones of gable buildings where the roof pitch is any value less than or equal to 27º, as these are the cases which were examined in this thesis. For any other building roof pitch angle, one can refer to the ASCE 7-10 specifications.

External pressure coefficient recommended values and zones are provided for the roof of gable buildings with a roof pitch greater than 7º and less than or equal to 27º in Figure 30.4-2B (ASCE 7-10). The notations from Figure 30.4-2B specify the dimension *a* to be, "10% of least horizontal dimension or 0.4h, whichever is smaller, but not less than either 4% of least horizontal dimension or 3 ft (0.9 m)". Where the

dimension *h* is determined by the mean roof height, except for the case where the eave height should be used when the roof pitch is less than or equal to 10º. The notations from Figure 30.4-1 for the wall zones use the same quotation for the dimension *a*. Note that the dimension *a* is measured on the projection of the roof onto a horizontal plane. An example is provided in Figure 3.9 showing the zones specified by Figure 30.4-2B applied to a gable building with a roof pitch greater than 7º and less than or equal to 27º. Similar application of the dimension *a* from Figure 3.8 should be applied for Figure 3.9.

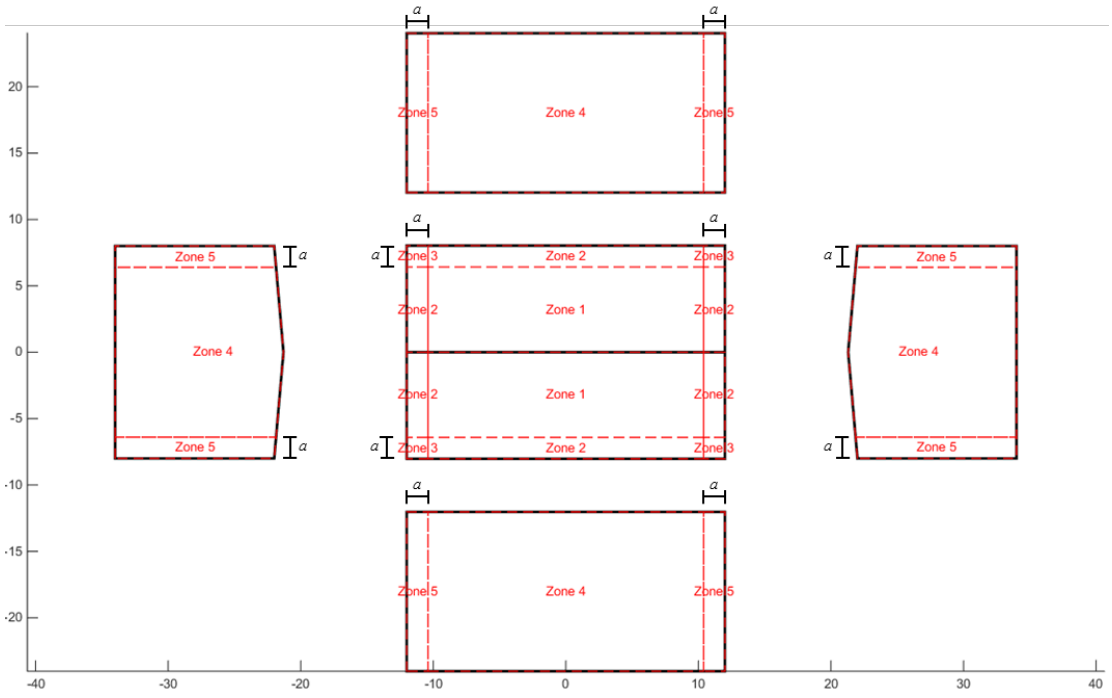

Figure 3.8: Zone layout for a gable building with roof pitch ≤ 7º (Figure 30.4-2A, ASCE 7-10)

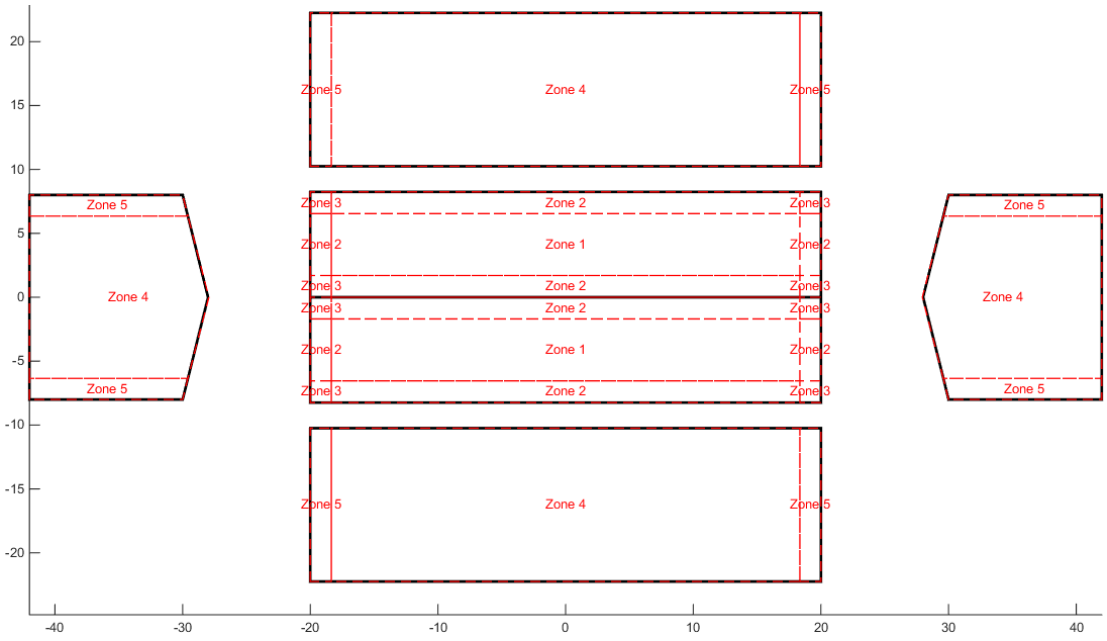

Figure 3.9: Zone layout for a gable building with 7º < Roof Pitch ≤ 27º (Figure 30.4-2B, ASCE 7-10)

Applying these ASCE 7-10 specific zones allows the sorting of external pressure coefficients into their respective zone plots for comparison with the external pressure coefficient charts. Overlaying the existing recommended external pressure coefficient values from ASCE 7-10's charts allows for direct comparison with the methodology's results.

Chapter 4: Results

4.1. Methodology Applied to Select Buildings from TPU's Low-Rise Building Wind Tunnel Database

The methodology discussed in Chapter 3 has been programmed to process any of the available gable buildings in TPU's low-rise building wind tunnel database, specifically case numbers 13 to 108 from Table 2.1. Analysis was performed on a select number of buildings which are listed in Table 4.1, and the results are presented subsequently. The buildings selected for analysis in this study are the same buildings which were analyzed in the Hagos et. al. (2014) study.

Table 4.1: Selected buildings for analysis from TPU's Database

Test Label TPU-#	Case Number (#)	Roof Type	Breadth B (m)	Depth D (m)	Eave height H0 (m)	Roof Pitch β (degrees)
TPU-1	61	Gable	16	24	12	4.8
TPU-2	93	Gable	16	40	12	4.8
TPU-3	95	Gable	16	40	12	14

The first gable building selected for analysis, labeled TPU-1, has the following dimensions: depth D = 24 m (78.74 ft), breadth B = 16 m (52.5 ft), eave height $H0$ = 12 m (39.37 ft), and a roof slope of β = 4.8 degrees. The second and third gable buildings selected, TPU-2 and TPU-3, have dimensions depth D = 40 m (131.23 ft), breadth B = 16 m (52.5 ft), eave height $H0$ = 12 m (39.37 ft), and roof slope of β = 4.8 and 14 degrees respectively.

Observing the distributions of the pressure tap locations along the surfaces of the buildings revealed that the pressure taps were irregularly spaced. Therefore, the Voronoi diagram provided substantial assistance as it was applied to each of the tested buildings to find the tributary areas of the irregularly spaced pressure taps. Plots of the

flattened building surfaces, along with the pressure tap locations represented by red circles and the tributary area boundaries represented by blue lines and blue circles, are shown for each of the studied buildings in Figure 4.1, Figure 4.2 and Figure 4.3.

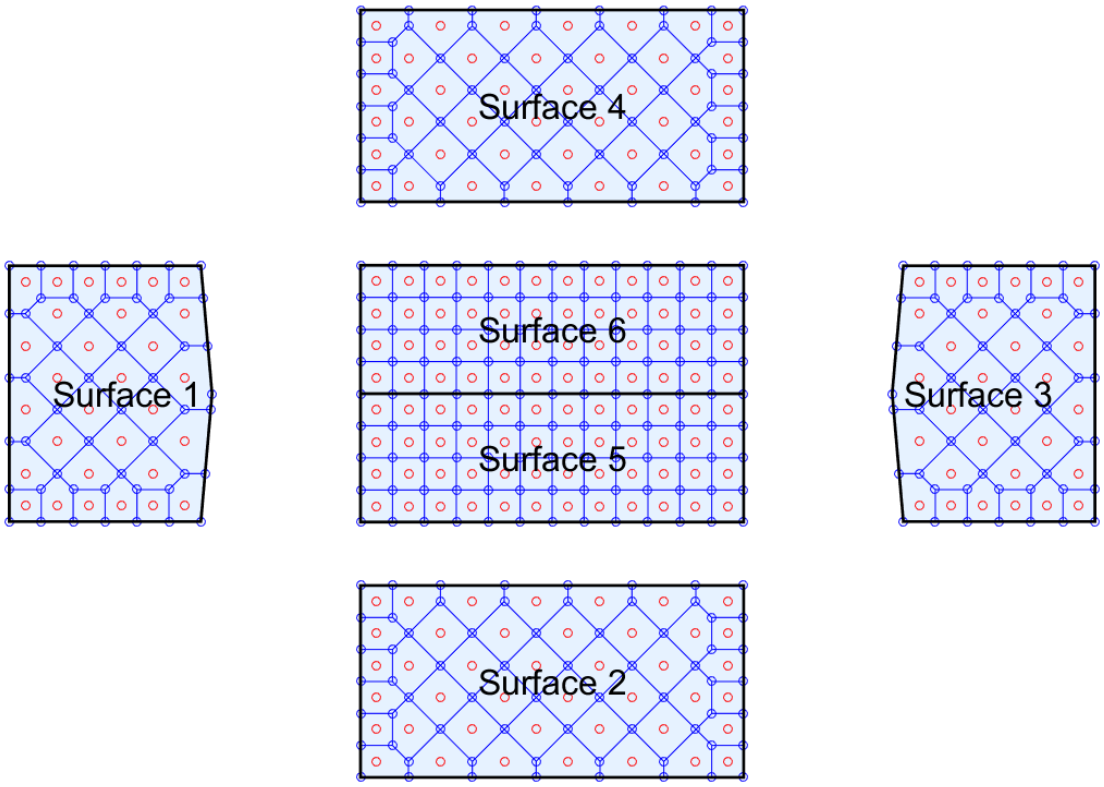

Figure 4.1: Plot of pressure tap locations and tributary areas for TPU-1

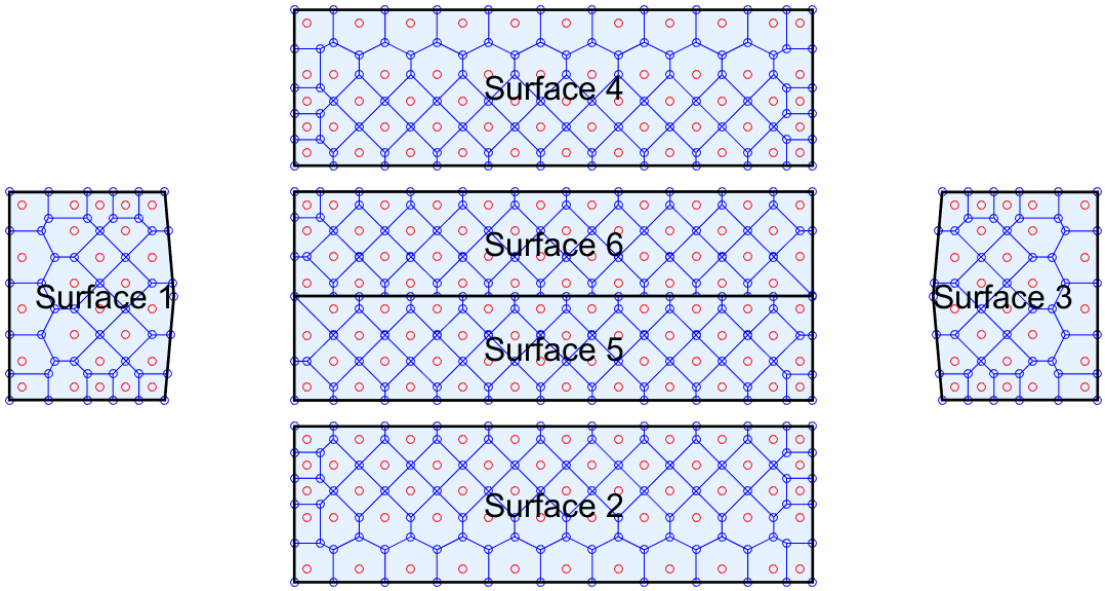

Figure 4.2: Plot of pressure tap locations and tributary areas for TPU-2

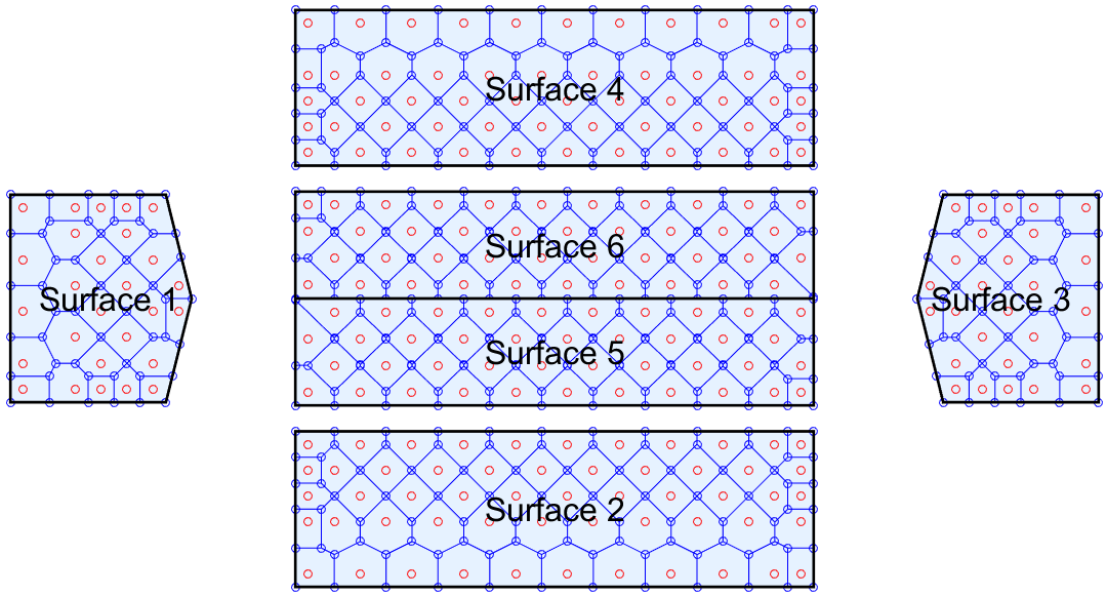

Figure 4.3: Plot of pressure tap locations and tributary areas for TPU-3

The next step for implementing the methodology involved deciding appropriate grid areas. As the majority of TPU's pressure taps are often spaced at 2 m on center, the smallest possible grid area was chosen as 2 m × 2 m. The largest possible grid area was selected as 7 m × 7 m. The grid areas are then incremented from 2 m × 2 m up to 7 m × 7 m, by values of 0.5 m. Likewise, the offset increments were also incremented

by 0.5 m in each direction. Using this distribution, the total number of grid area combinations is 9,801 (e.g., 9,801 sample area grids, each grid with a unique grid area/offset combination). A similar example for obtaining all grid area combinations is provided in Chapter 3.

After compiling the list of grid area combinations, the next step was to determine the peak external pressure coefficient for each applicable grid area. The first grid area combination was selected, starting with 2 m × 2 m and an offset of 0 m in the x- and y-direction. The calculation of the pressure time series values are area-weighted averaged into their corresponding grid areas from their relative tributary areas. Next, the peak pressure coefficient of each grid area is estimated using the Maxminest function (Main, 2011). As required by the peak estimating function, the calculation for the duration ratio D_R is shown in Eq. (4.1), where the duration for the storm of interest is the hourly wind storm 3600 s, and the full-scale duration of the measured TPU record is 600 s. The duration ratio D_R resulted to 6.0 for each of the TPU studies performed.

$$D_R = \frac{\text{duration of storm of interest}}{\text{full-scale duration of measured record}} = \frac{3600}{600} = 6.0 \qquad (4.1)$$

Applying the peak estimation function with the duration ratio provides the maximum and minimum peak pressure coefficients for each of the applicable grid areas. This process is then repeated for the pressure time series data from each of the other wind directions. After each of the wind directions have been analyzed, the results are stored and the method is repeated for the following grid area combination, 2 m × 2 m with an offset of 0 m in the x-direction and 0.5 m in the y-direction, and for all remaining grid area combinations thereafter.

Applying the calculation of peak pressure coefficients to the buildings studied for each grid area and each wind direction allows for the determination of the worst case peak envelope plot. The minimum and maximum peak pressure coefficients are presented from TPU-1 for each of the wind angles θ tested (0, 15, 30, 45, 60, 75 and 90 degrees) in Figure 4.4 thru Figure 4.17 to demonstrate this procedure. For these figures, a grid area combination of 2 m × 2 m was selected with no offset. Using these worst case peak minimum and maximum values, the plot of the envelope, considering all wind directions, is produced and is revealed subsequently in Figure 4.18. Please take into consideration that the color bar legend is different for each of the following figures.

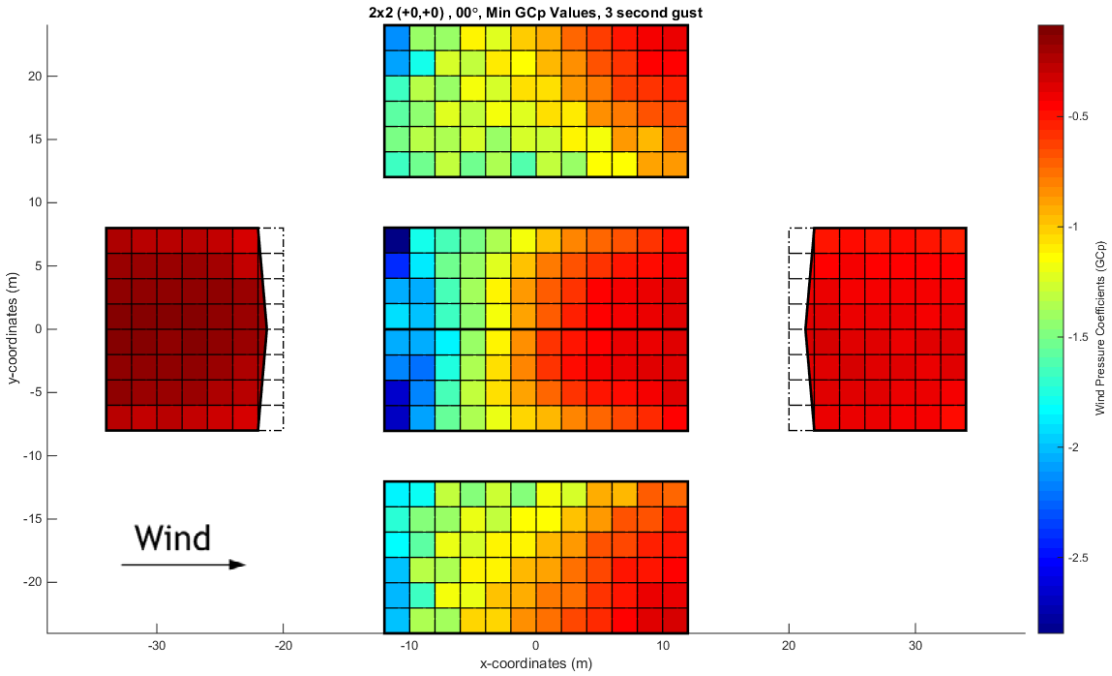

Figure 4.4: Peak minimum external pressure coefficients for TPU-1 with wind angle $\theta = 0^{o}$

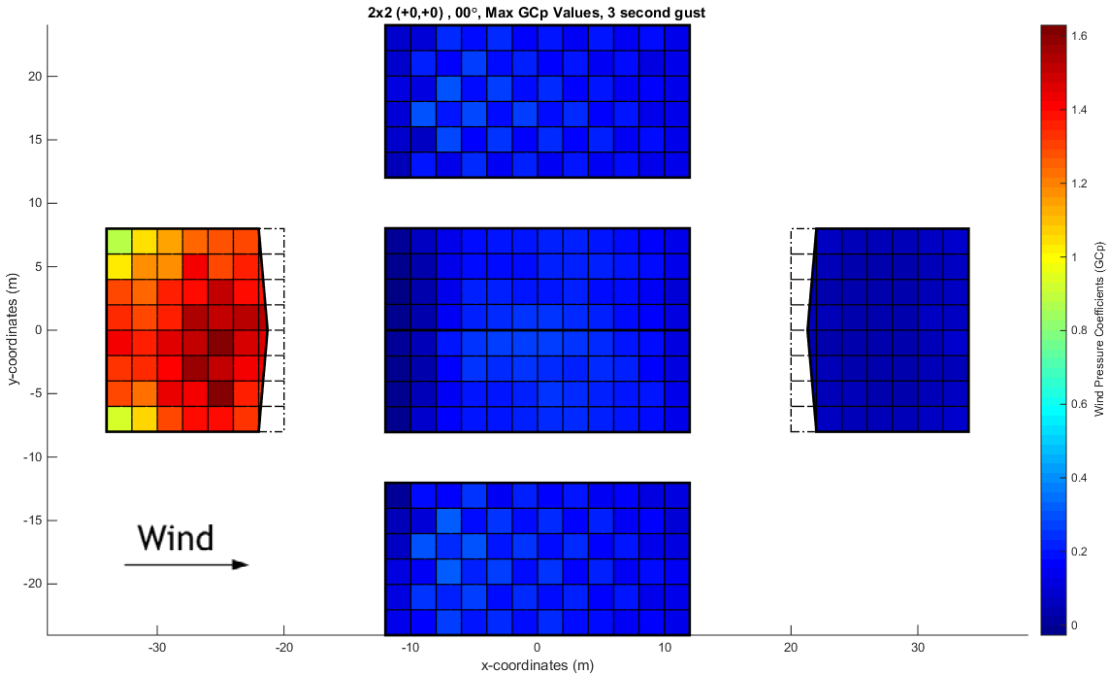

Figure 4.5: Peak maximum external pressure coefficients for TPU-1 with wind angle $\theta = 0^{o}$

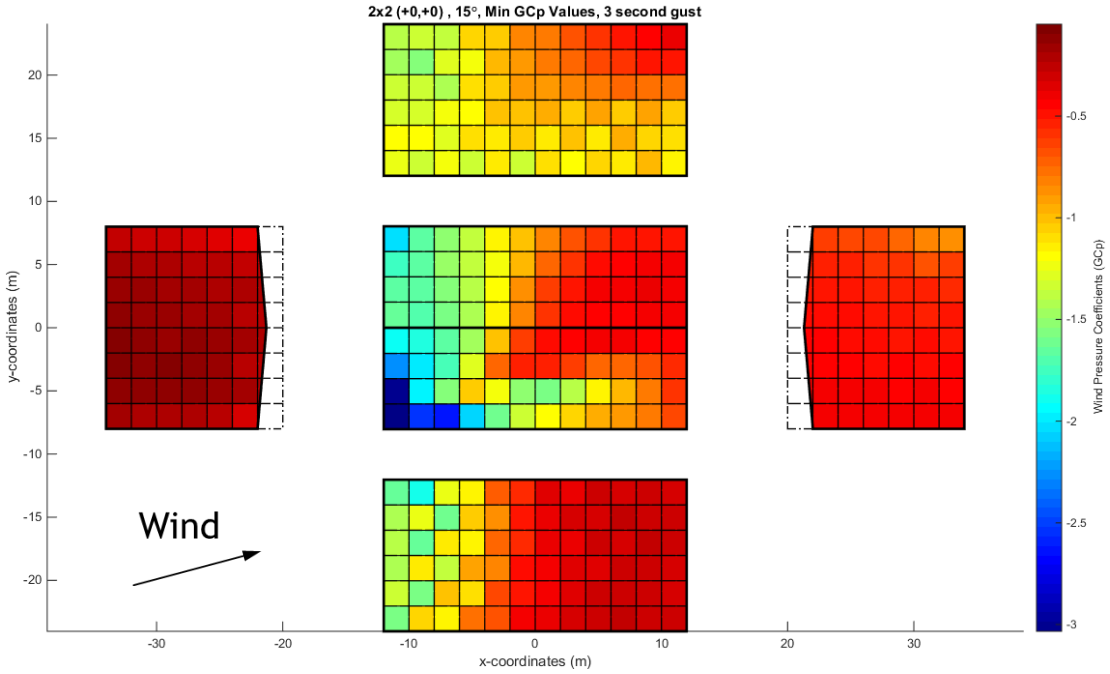

Figure 4.6: Peak minimum external pressure coefficients for TPU-1 with wind angle $\theta = 15^{o}$

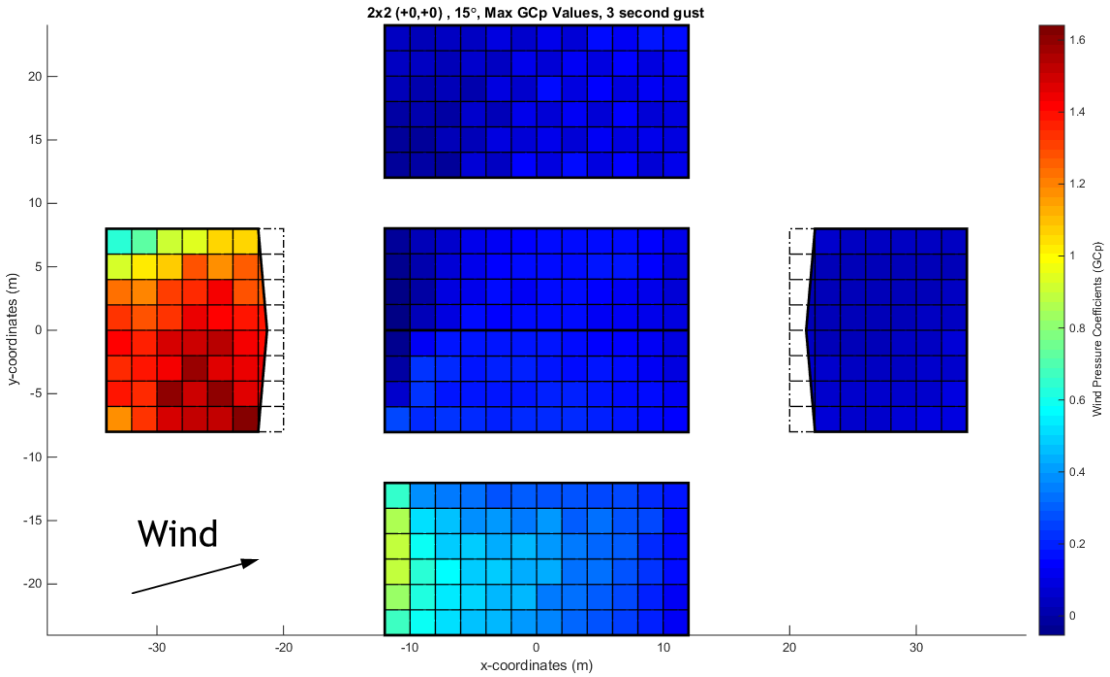

Figure 4.7: Peak maximum external pressure coefficients for TPU-1 with wind angle $\theta = 15^{o}$

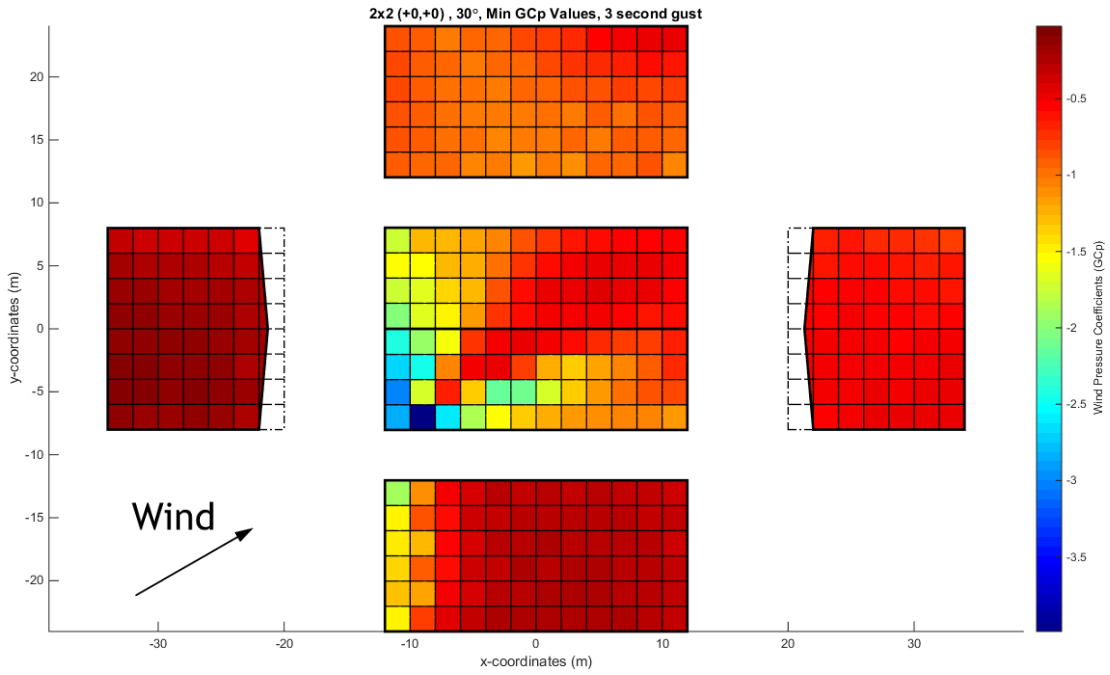

Figure 4.8: Peak minimum external pressure coefficients for TPU-1 with wind angle $\theta = 30^{o}$

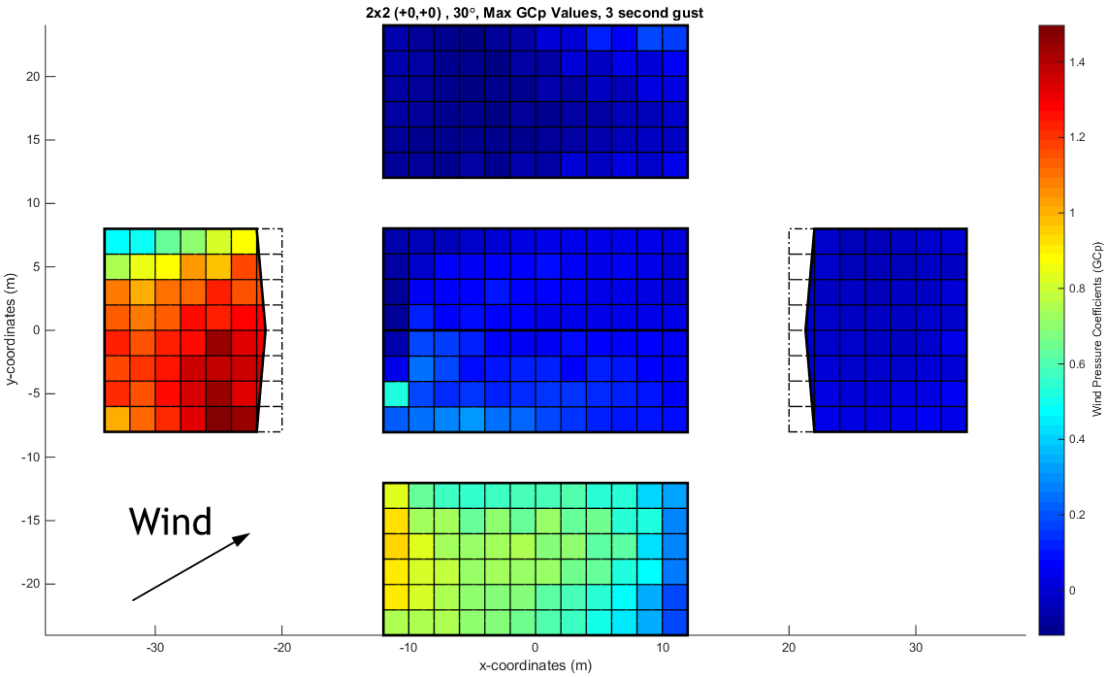

Figure 4.9: Peak maximum external pressure coefficients for TPU-1 with wind angle $\theta = 30^{o}$

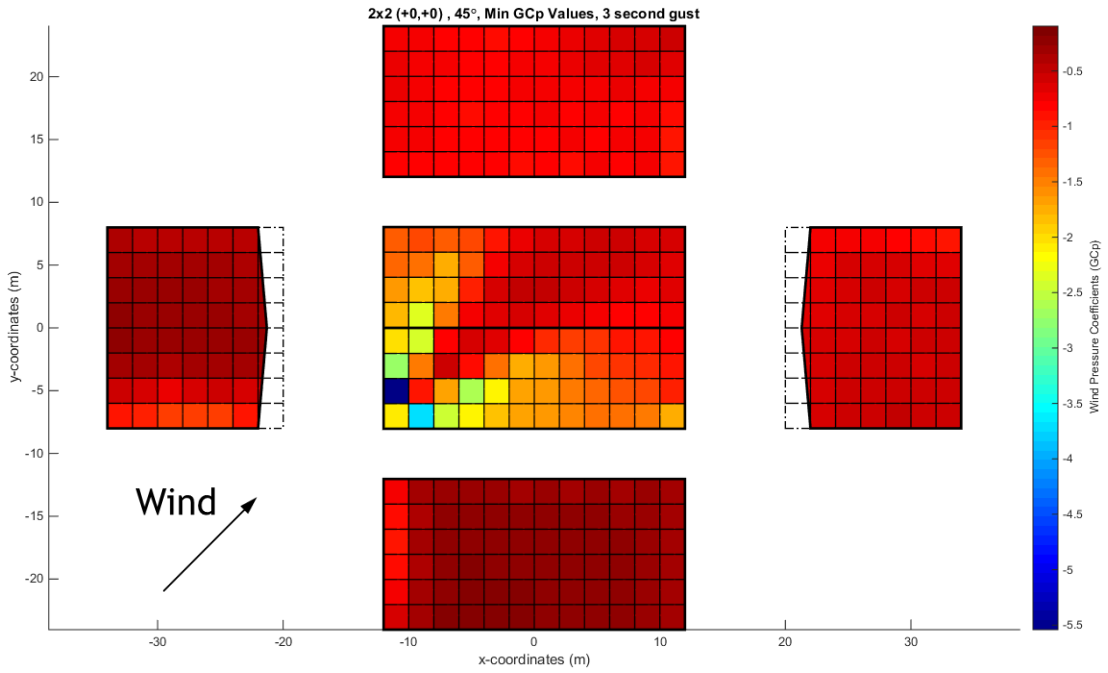

Figure 4.10: Peak minimum external pressure coefficients for TPU-1 with wind angle $\theta = 45^{o}$

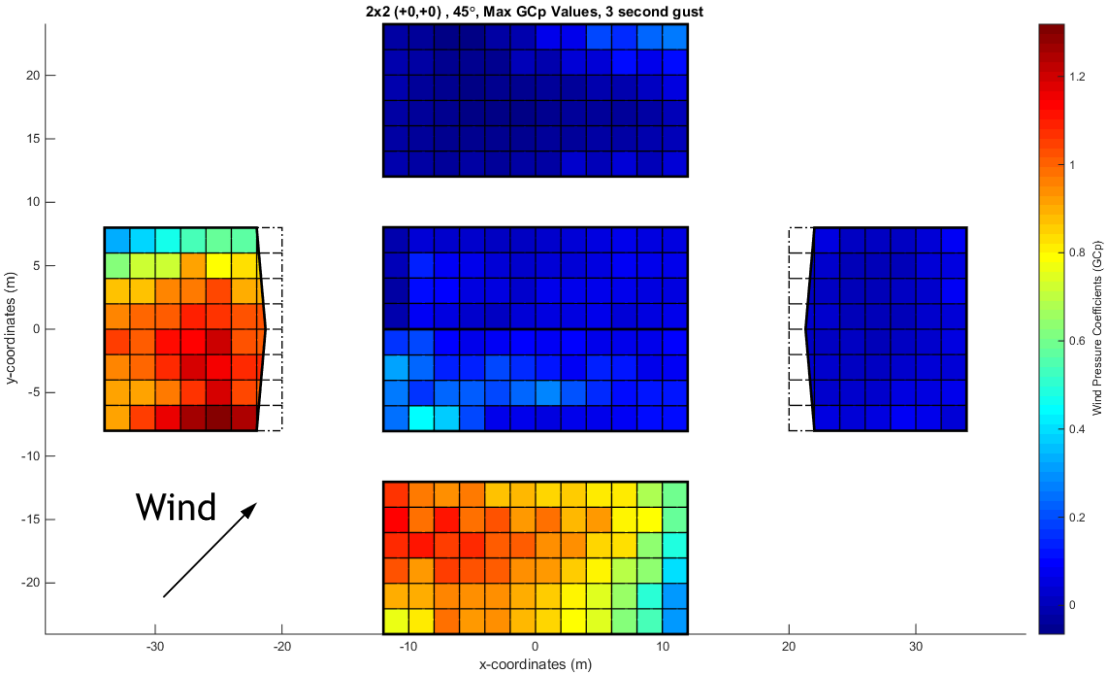

Figure 4.11: Peak maximum external pressure coefficients for TPU-1 with wind angle $\theta = 45^{o}$

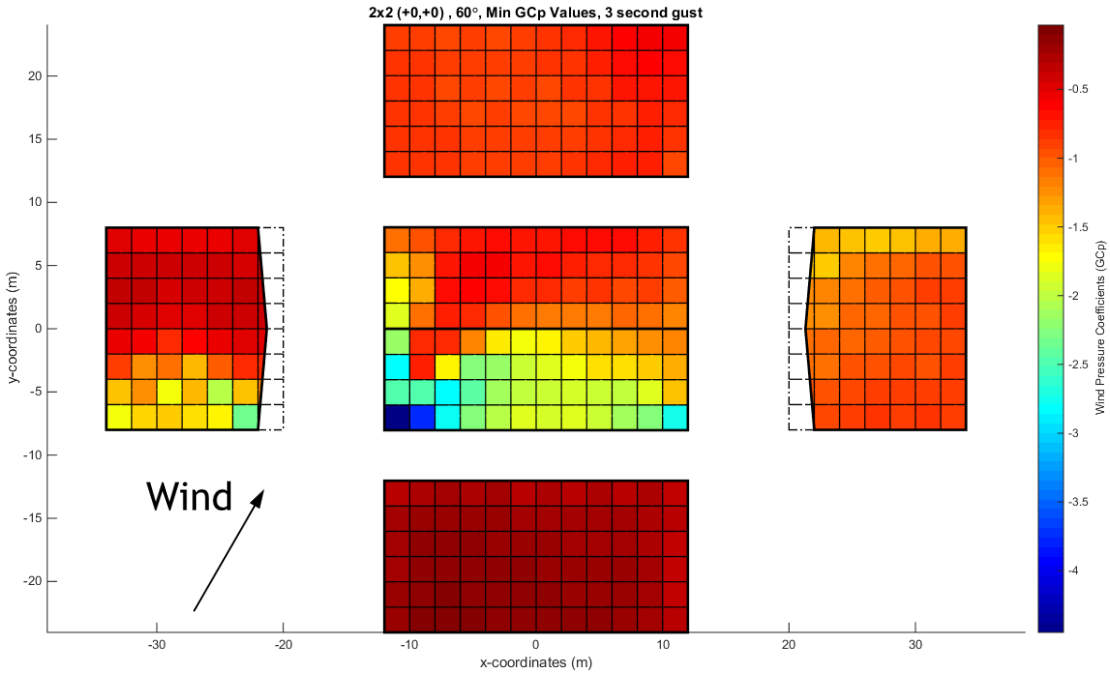

Figure 4.12: Peak minimum external pressure coefficients for TPU-1 with wind angle $\theta = 60^{o}$

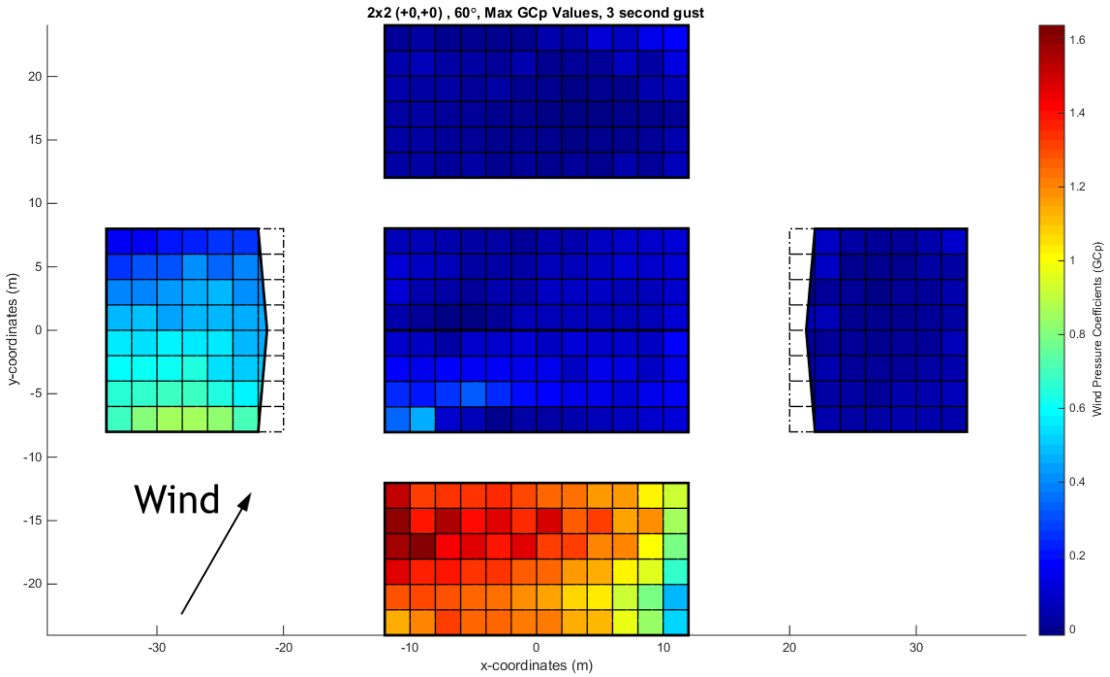

Figure 4.13: Peak maximum external pressure coefficients for TPU-1 with wind angle $\theta = 60^{o}$

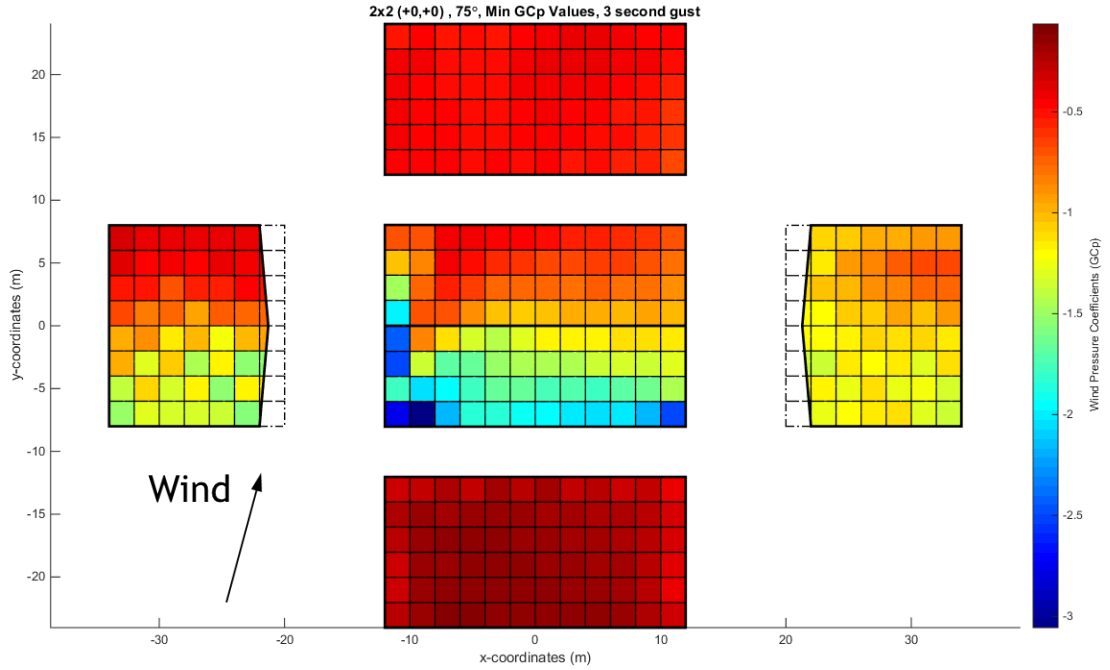

Figure 4.14: Peak minimum external pressure coefficients for TPU-1 with wind angle $\theta = 75^{o}$

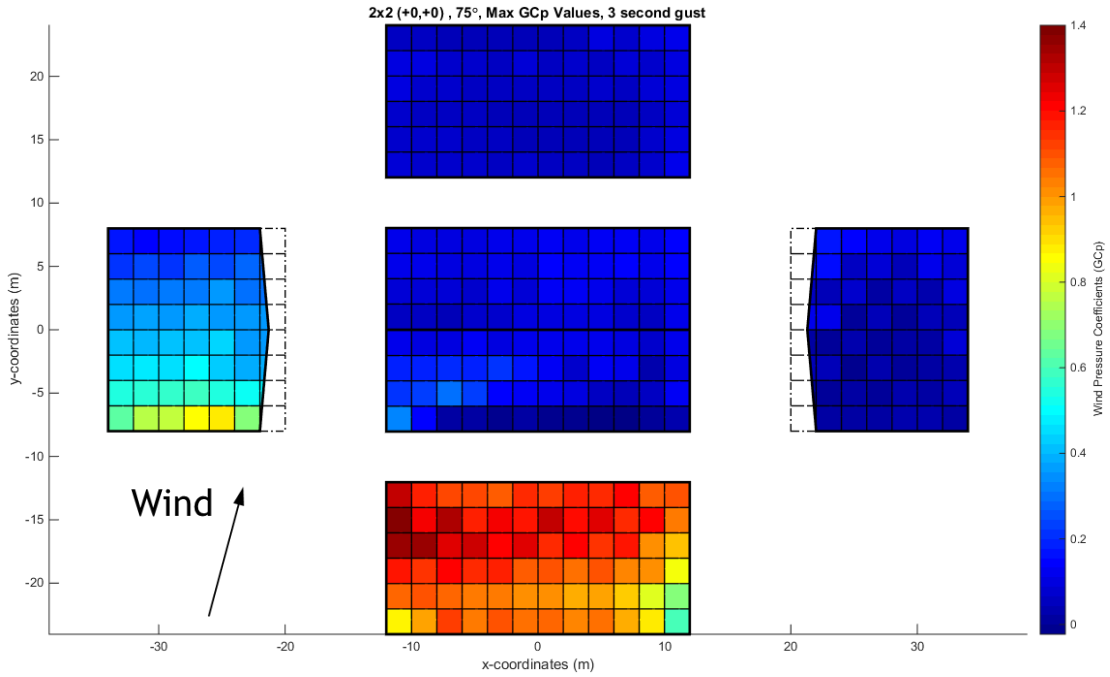

Figure 4.15: Peak maximum external pressure coefficients for TPU-1 with wind angle $\theta = 75^{o}$

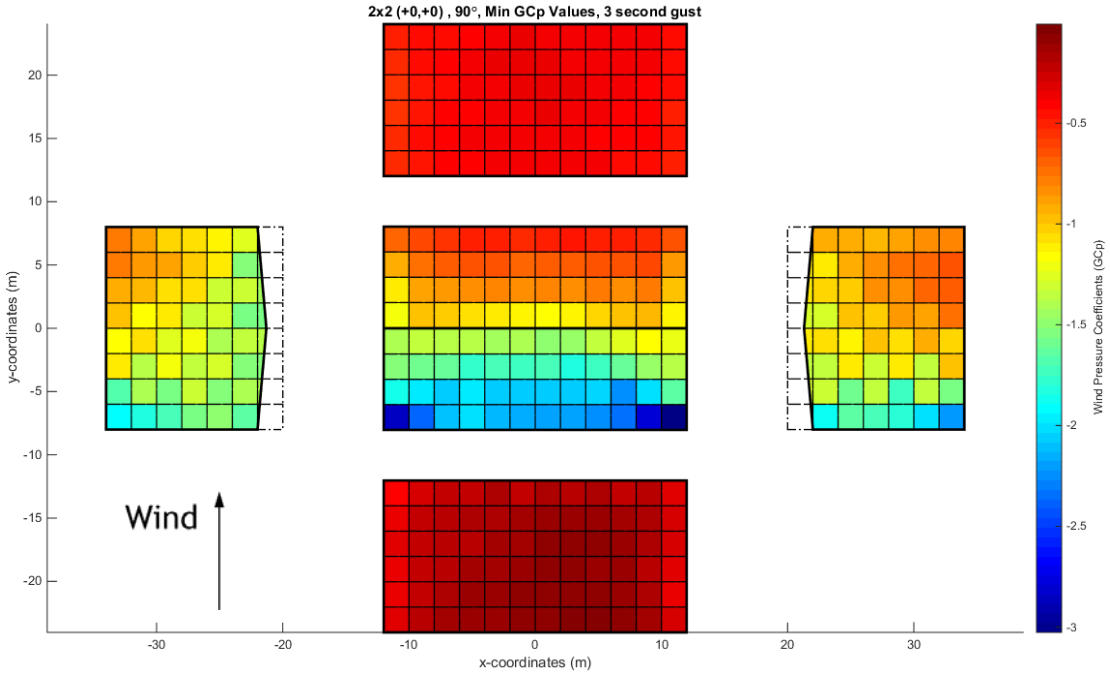

Figure 4.16: Peak minimum external pressure coefficients for TPU-1 with wind angle $\theta = 90^{o}$

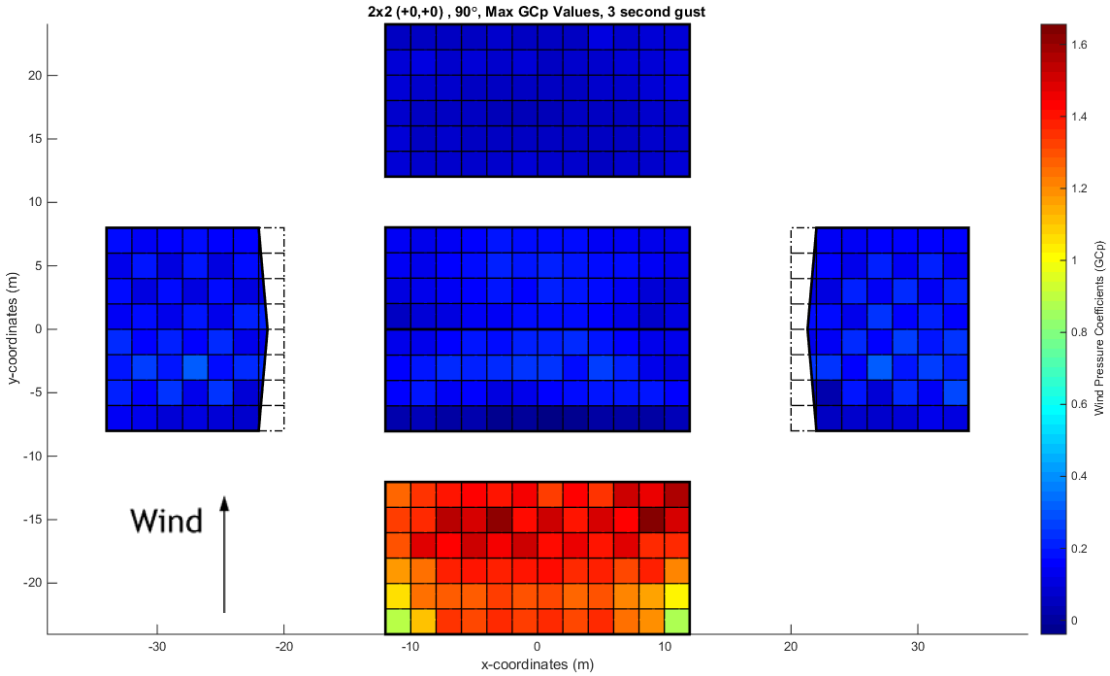

Figure 4.17: Peak maximum external pressure coefficients for TPU-1 with wind angle $\theta = 90^{o}$

Assembling the worst case peak pressure coefficients from all available wind directions, using either the minimum peaks or the maximum peaks, produces the worst case plot of the building envelope for each grid area. The plots of the minimum and maximum envelope peak external wind pressure coefficients for a grid size of 2 m × 2 m with no offset are shown for: TPU-1 in Figure 4.18 and Figure 4.19, TPU-2 in Figure 4.20 and Figure 4.21, and TPU-3 in Figure 4.22 and Figure 4.23.

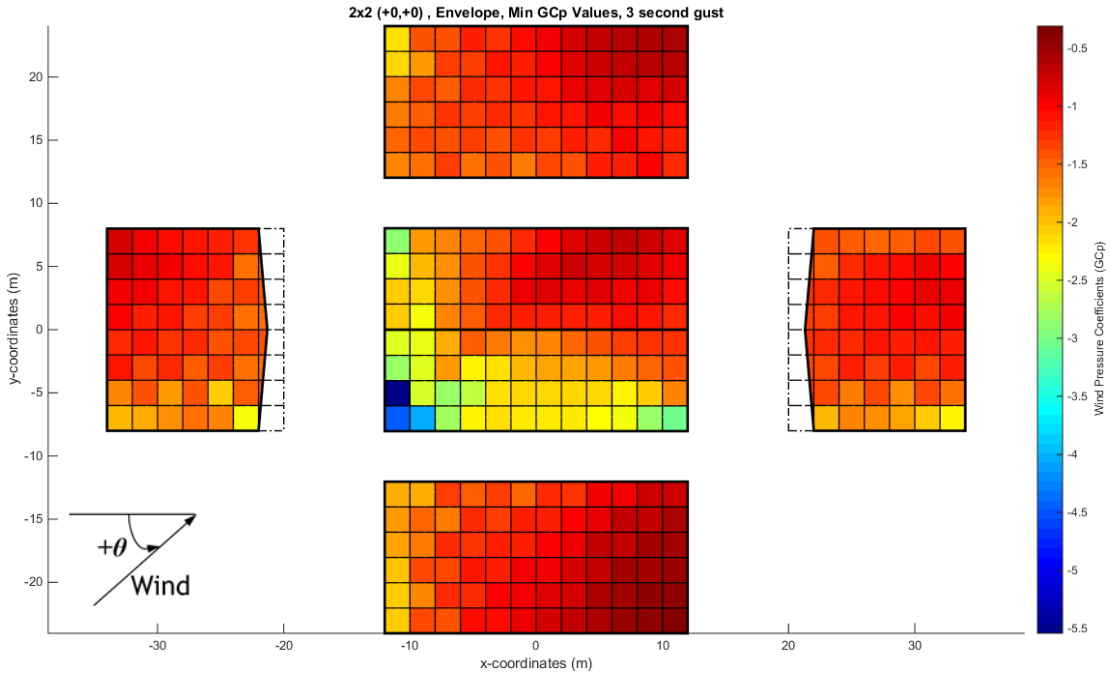

Figure 4.18: TPU-1, Envelope of minimum peak external pressure coefficients for 2 m × 2 m grid area (no offset)

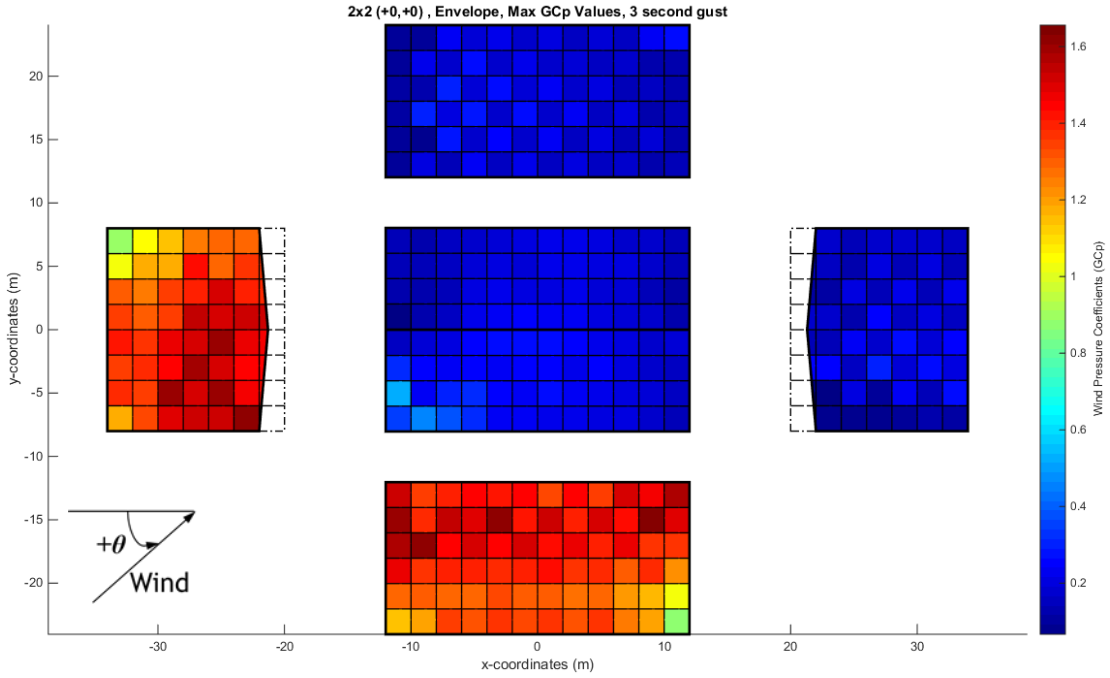

Figure 4.19: TPU-1, Envelope of maximum peak external pressure coefficients for 2 m × 2 m grid area (no offset)

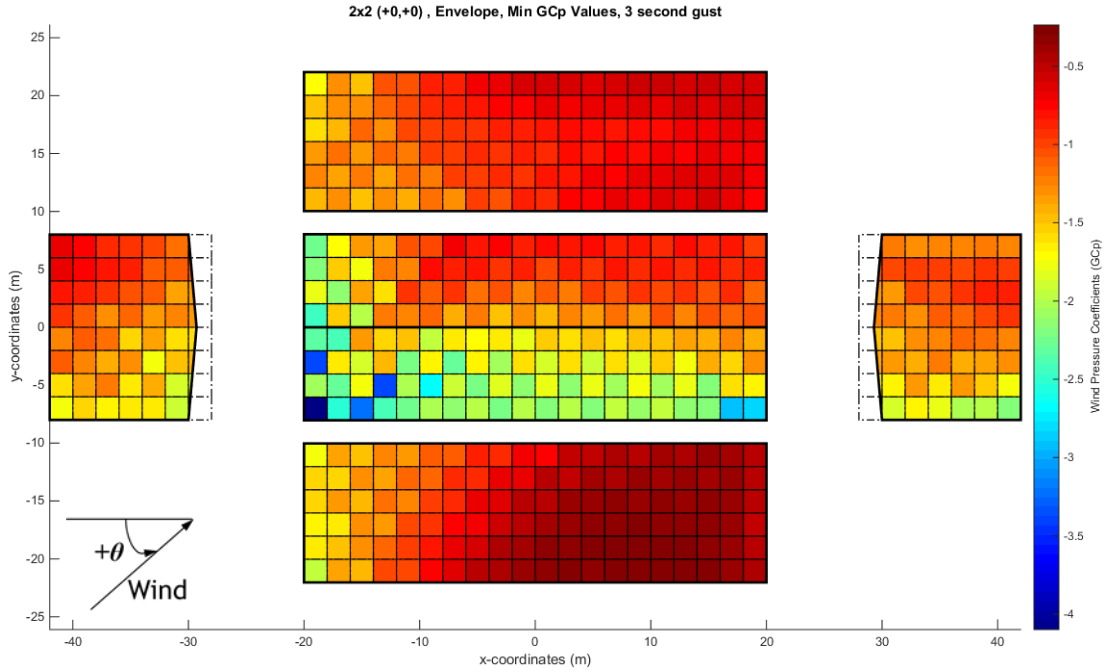

Figure 4.20: TPU-2, Envelope of minimum peak external pressure coefficients for 2 m × 2 m grid area (no offset)

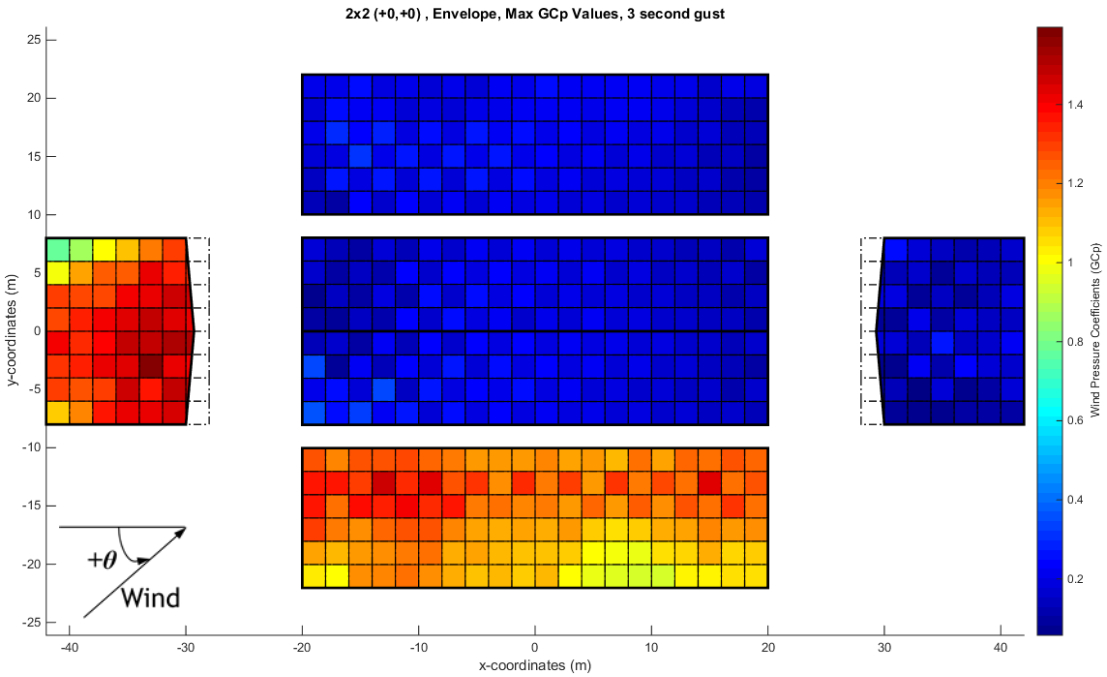

Figure 4.21: TPU-2, Envelope of maximum peak external pressure coefficients for 2 m × 2 m grid area (no offset)

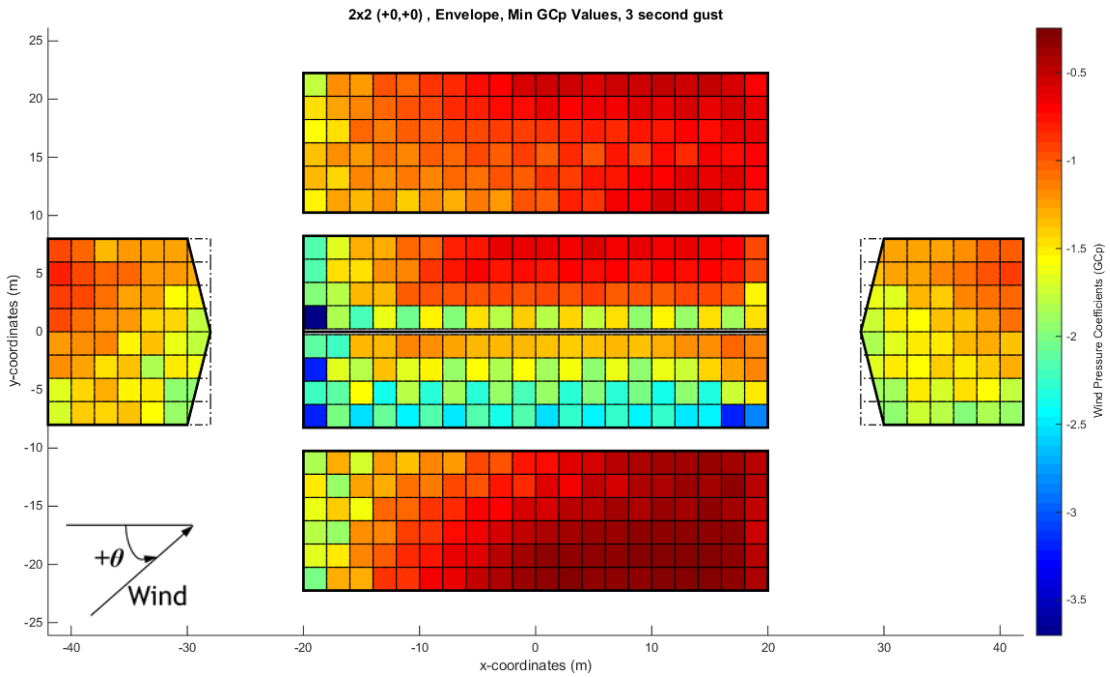

Figure 4.22: TPU-3, Envelope of minimum peak external pressure coefficients for 2 m × 2 m grid area (no offset)

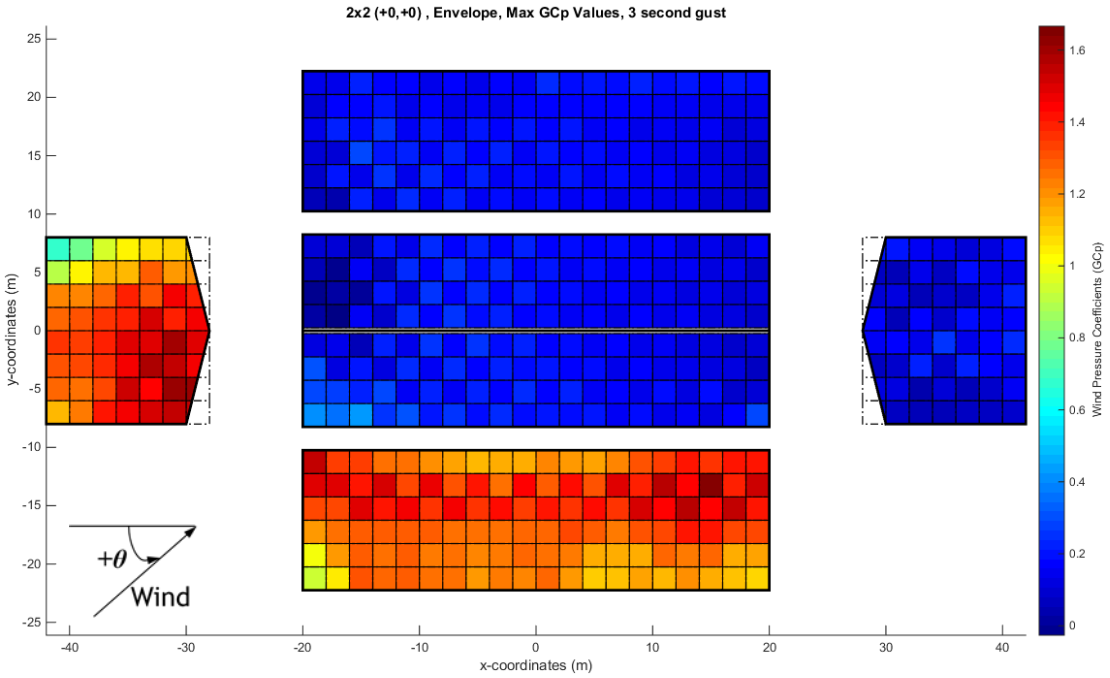

Figure 4.23: TPU-3, Envelope of maximum peak external pressure coefficients for 2 m × 2 m grid area (no offset)

Following the calculation of the envelope peak wind pressure coefficients, the building was separated into zones to compare the results with the ASCE 7-10 external pressure coefficient charts. The selected buildings TPU-1 and TPU-2 correspond to Figure 30.4-2A of ASCE 7-10 (External Pressure Coefficients GC_p for Enclosed and Partially Enclosed Buildings with Gable Roof of Slope 7º or less), while TPU-3 corresponds to Figure 30.4-2B (External Pressure Coefficients GC_p for Enclosed and Partially Enclosed Buildings with Gable Roof of Slope greater than 7º and less than or equal to 27º). Notice that TPU-3 contains a slightly different zone layout than TPU-1 and TPU-2. Applying the zoning specifications to the selected buildings yields a = 1.61 m for TPU-1 and TPU-2, and a = 1.65 m for TPU-3. The zones are then demonstrated in Figure 4.24 for TPU-1, Figure 4.25 for TPU-2, and Figure 4.26 for TPU-3.

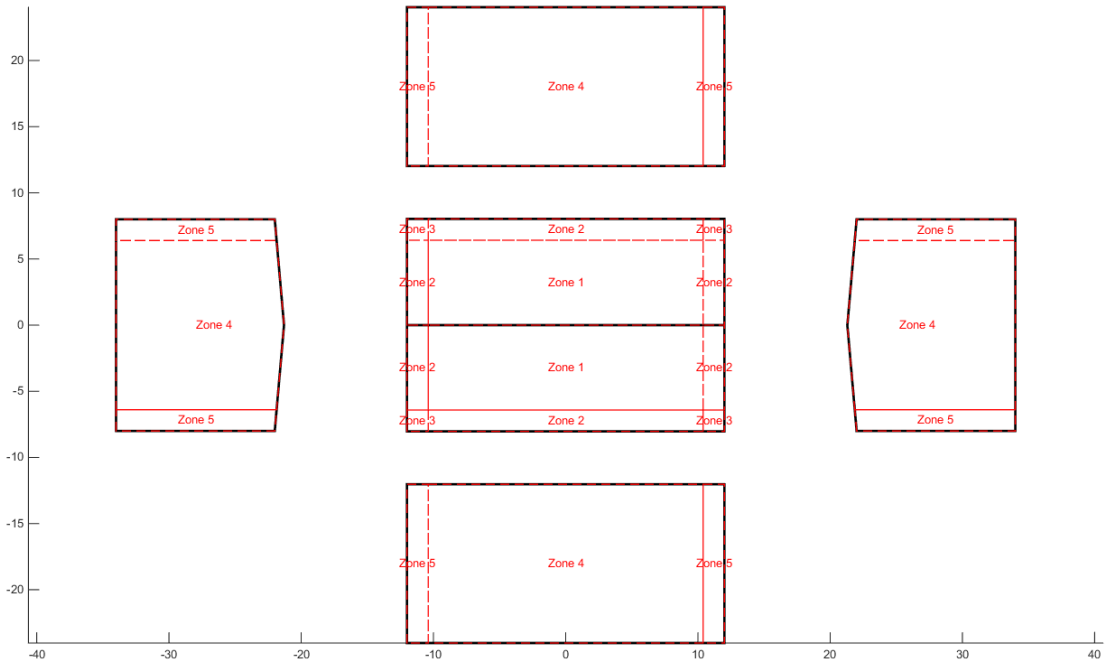

Figure 4.24: Applied zones for TPU-1

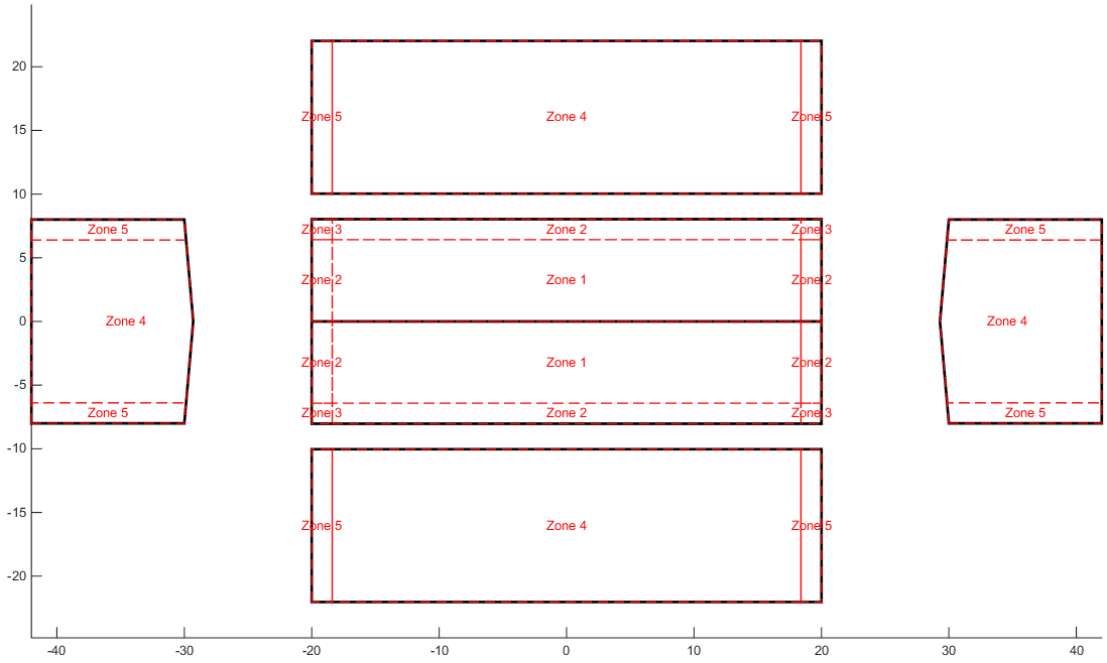

Figure 4.25: Applied zones for TPU-2

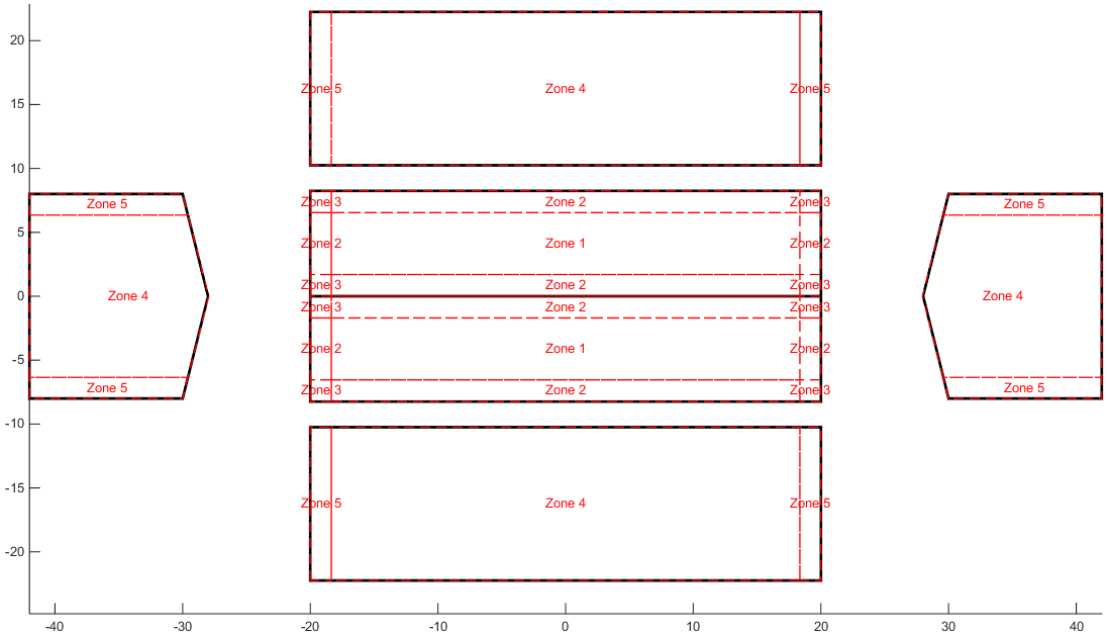

Figure 4.26: Applied zones for TPU-3

The peak wind pressure coefficients were assigned to their respective zones and the plots of the results are provided in Figure 4.27 for TPU-1, Figure 4.28 for TPU-2, and Figure 4.29 for TPU-3. In these plots, the red data points represent the negative

(suction) peak wind pressure coefficients, while the blue data points represent the positive (into the building) peak wind pressure coefficients. Additionally, the current ASCE 7-10 specifications for positive and negative external wind pressure coefficients were superposed to the plots using solid black lines. As the TPU database is limited by the smallest tap tributary areas of 2 m × 2 m, partial tributary areas must be considered to be able to populate zone 3 (corner regions) which have dimensions smaller than 2 m × 2 m for the buildings considered. To accommodate the narrow zones and coarse tap spacing, a decision was made to accept grid areas if at least 50% of the grid area falls within the zone. This method of accepting a grid area into a zone should not be confused with the previous decision to discard any partial grid areas which fell outside of the building boundaries. This rule for accepting grid areas if 50% of the grid area falls within the zone was applied as needed for edge zones 2, 3, and 5. However, this rule was not applied for interior zones 1 and 4, as the interior zones are not limited by narrow zone requirements.

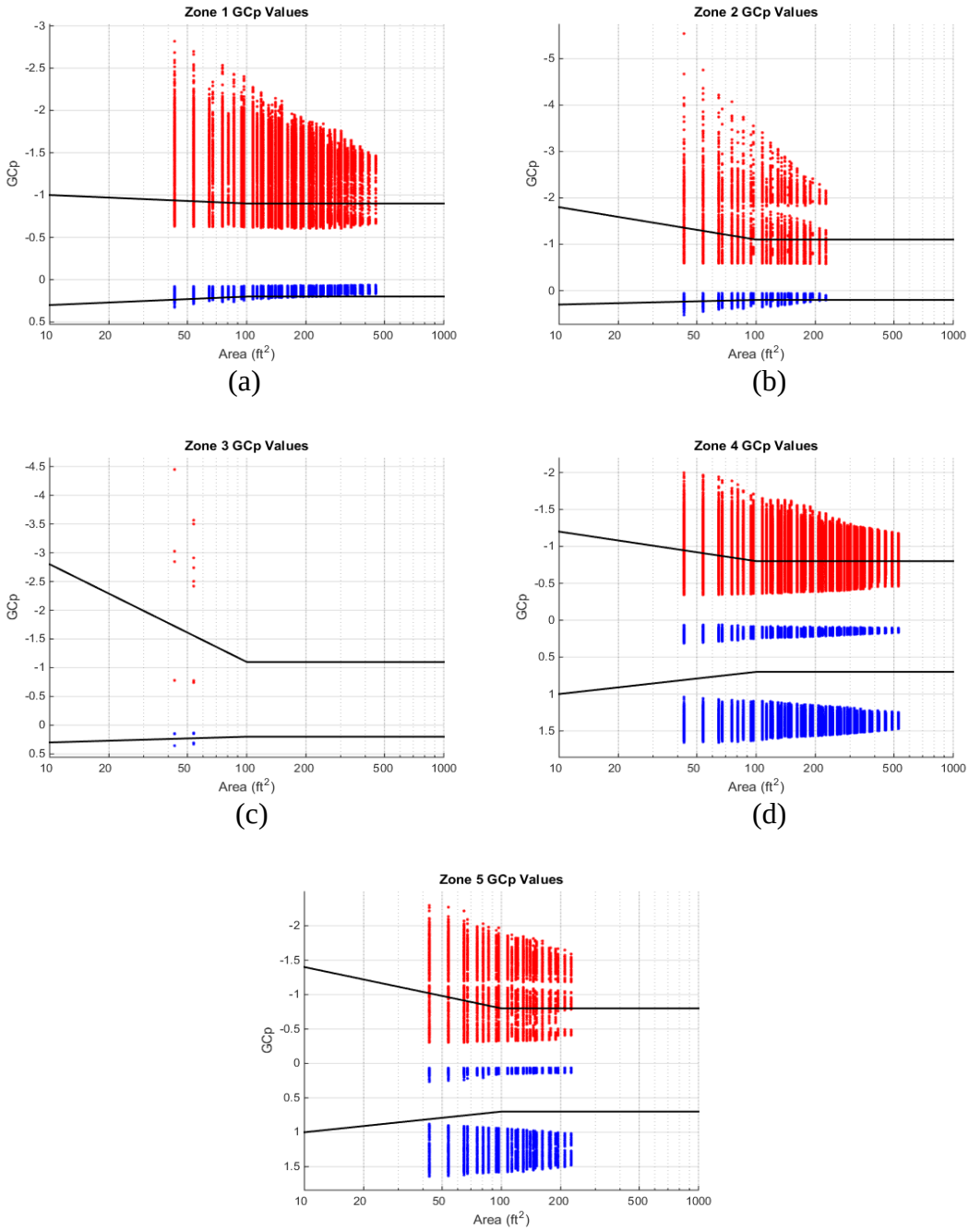

Figure 4.27: External pressure coefficients by respective zone for TPU-1

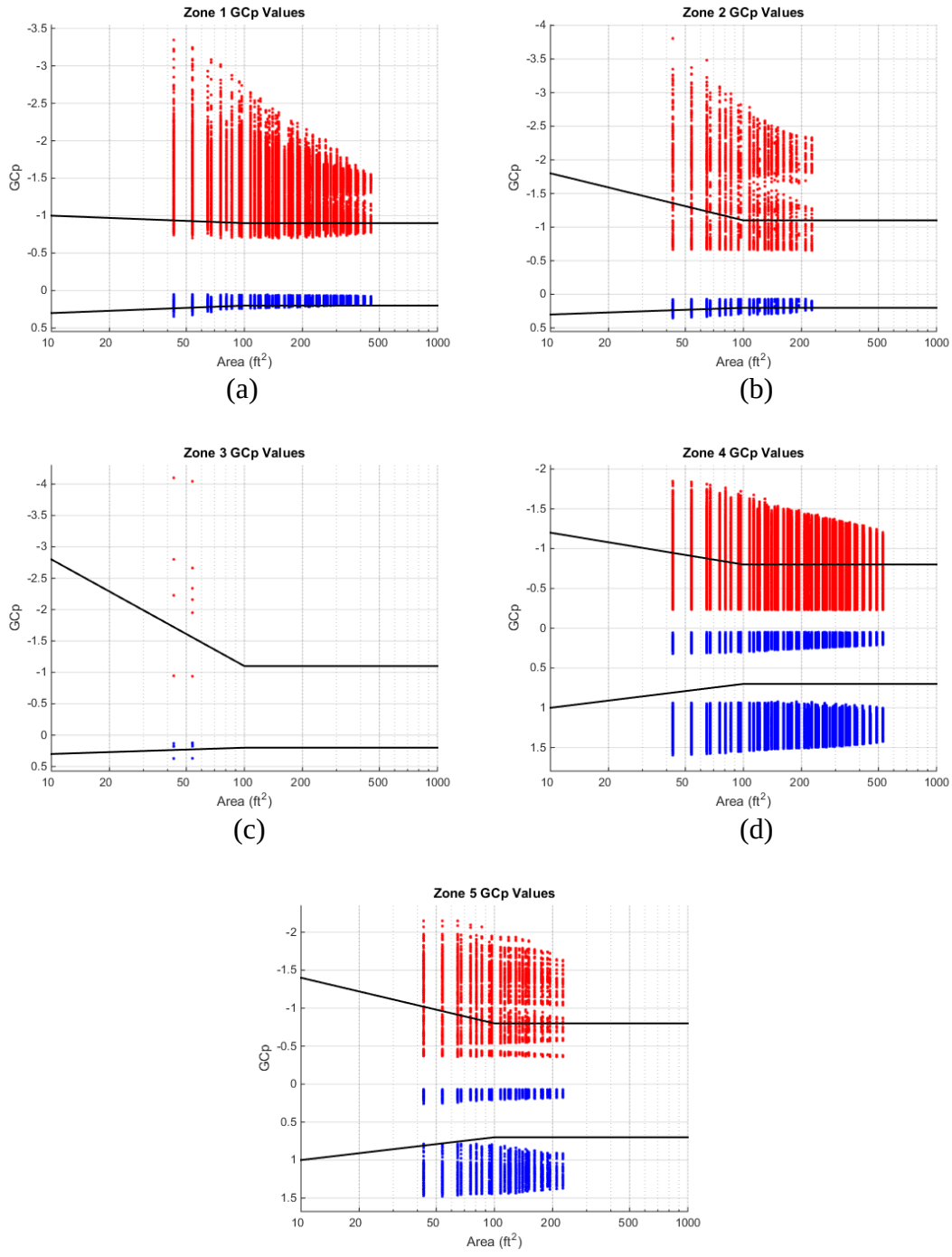

Figure 4.28: External pressure coefficients by respective zone for TPU-2

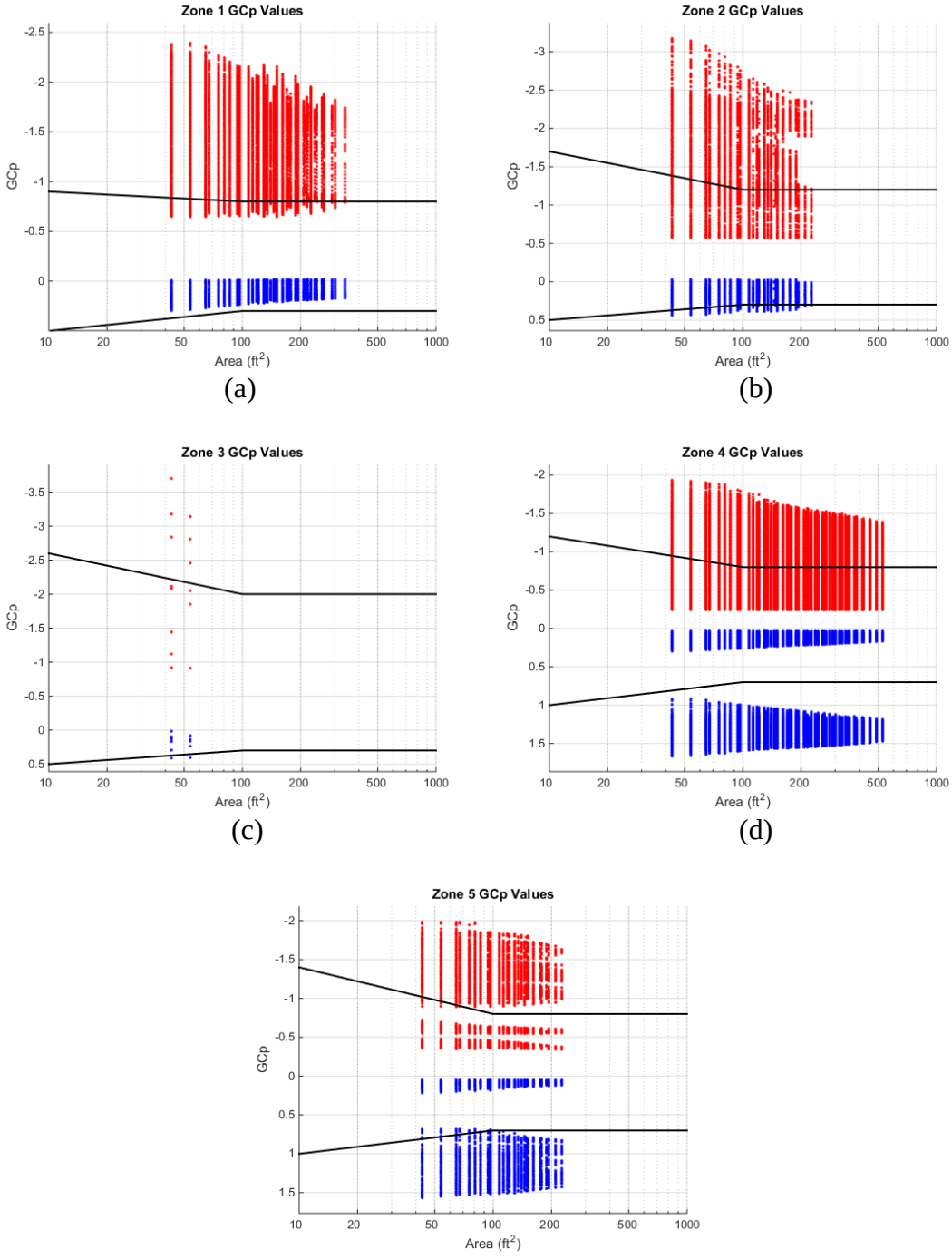

Figure 4.29: External pressure coefficients by respective zone for TPU-3

To understand the direction of the wind influencing the worst case values for the minimum and maximum envelopes, plots were developed which provide this information. This is not included as part of the methodology, as it is not required for

the calculation of the external pressure coefficients, but was simply a separate evaluation performed for analysis of the data. Plots were developed which provide the direction of the worst case wind angle θ, tested at 15 degree increments between 0 and 90 degrees, for each grid area with regards to either the maximum or minimum pressure values. The plot of the minimum and maximum wind directions for a 2 m × 2 m grid area with no offset is presented for TPU-1 in Figure 4.30 and Figure 4.31, for TPU-2 in Figure 4.32 and Figure 4.33, and for TPU-3 in Figure 4.34 and Figure 4.35.

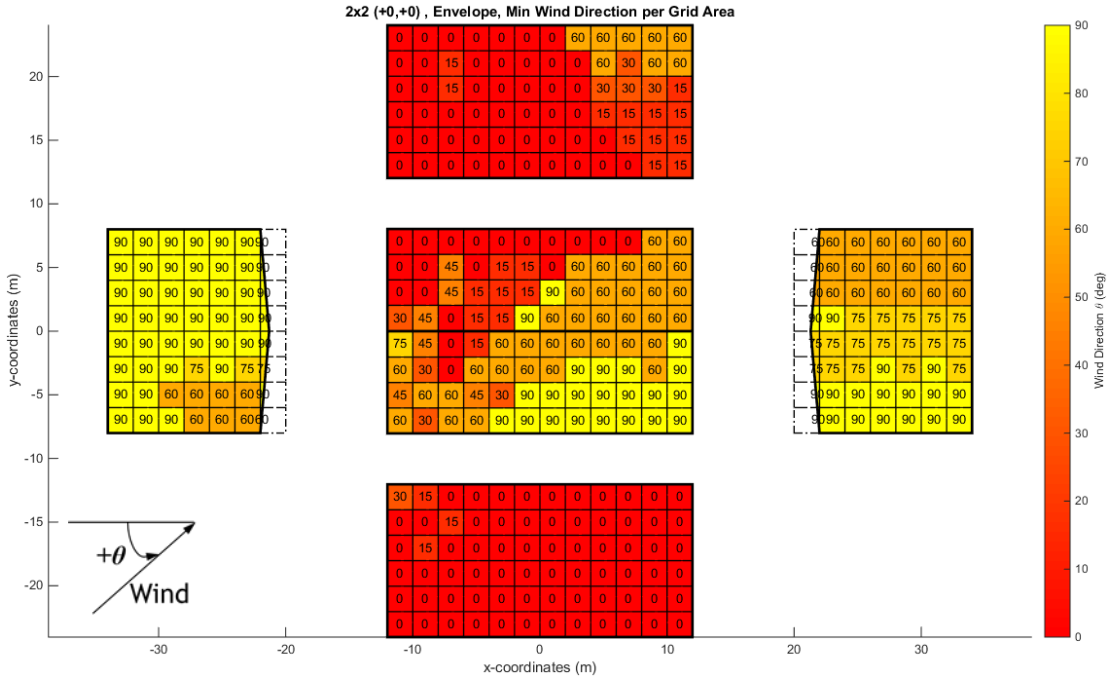

Figure 4.30: Worst case wind angles for the minimum pressures of TPU-1

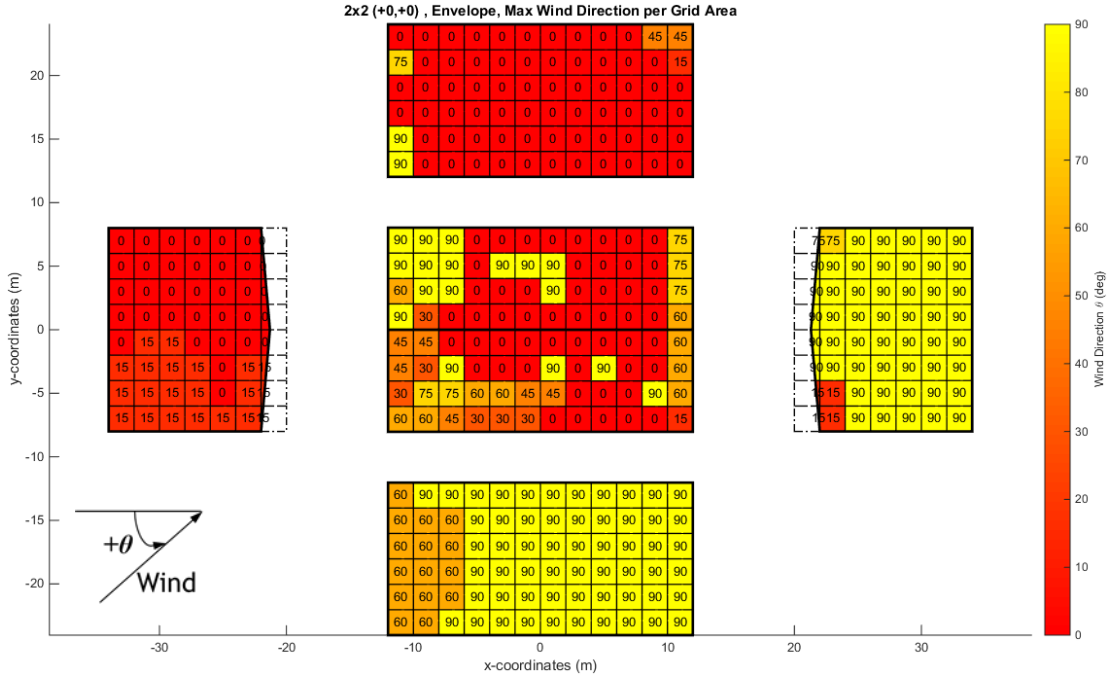

Figure 4.31: Worst case wind angles for the maximum pressures of TPU-1

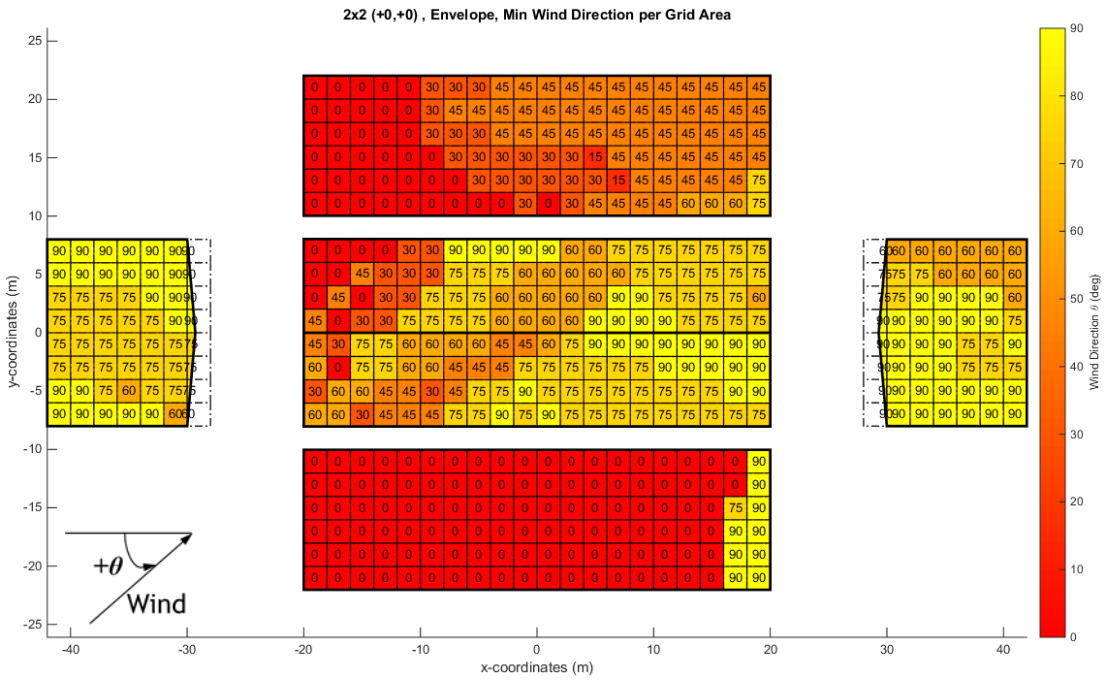

Figure 4.32: Worst case wind angles for the minimum pressures of TPU-2

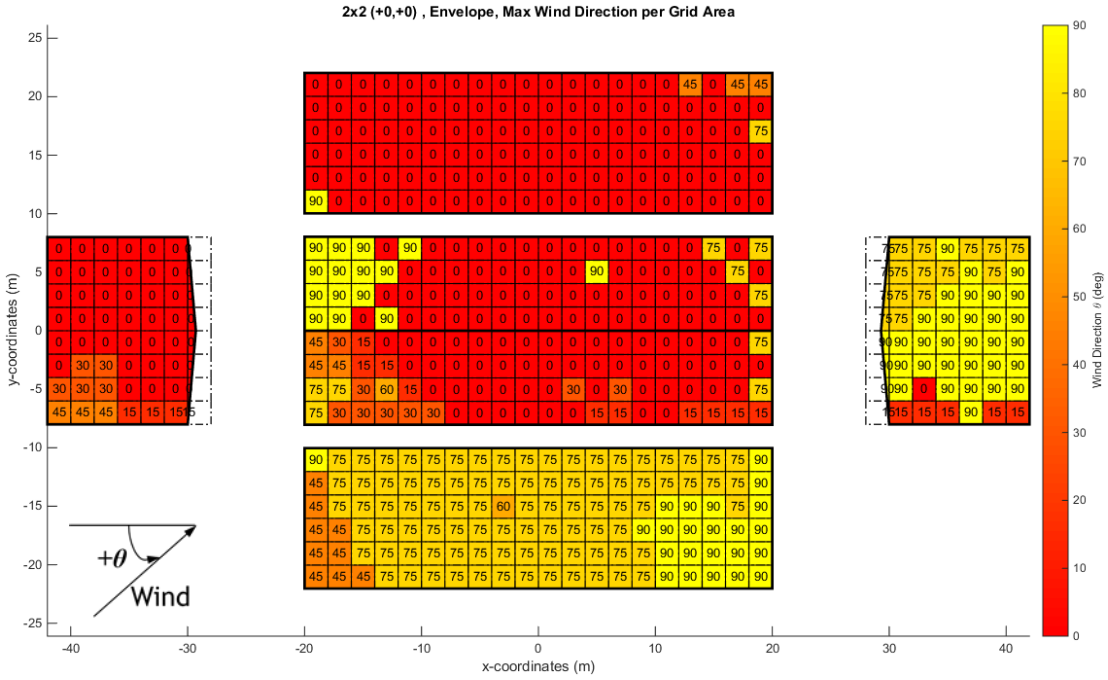

Figure 4.33: Worst case wind angles for the maximum pressures of TPU-2

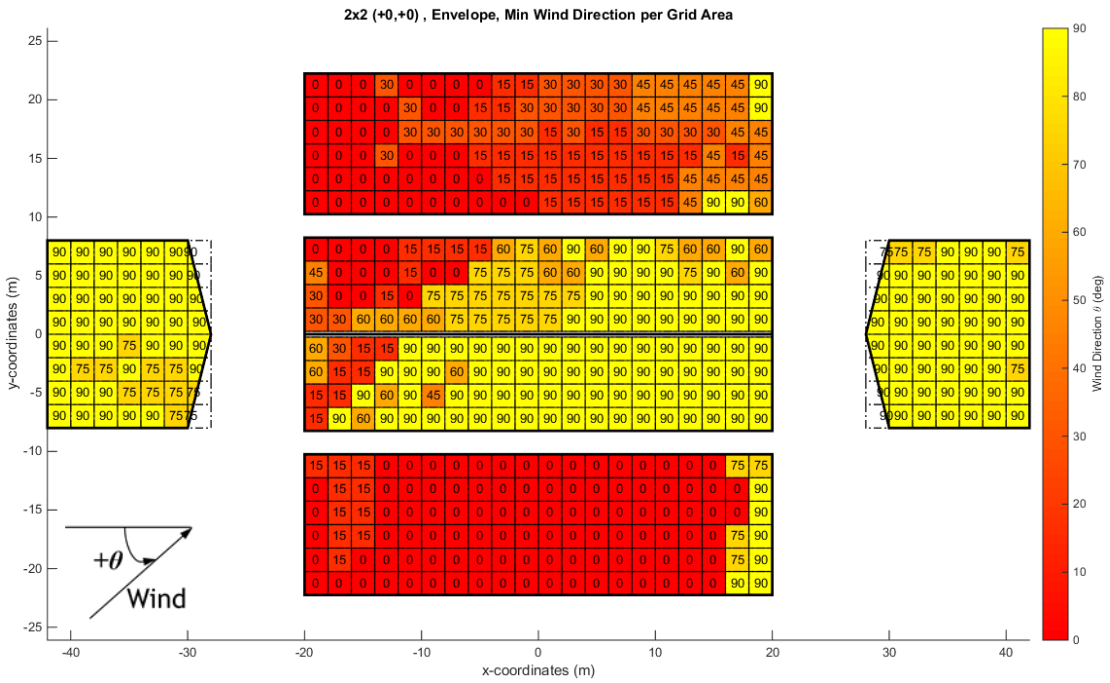

Figure 4.34: Worst case wind angles for the minimum pressures of TPU-3

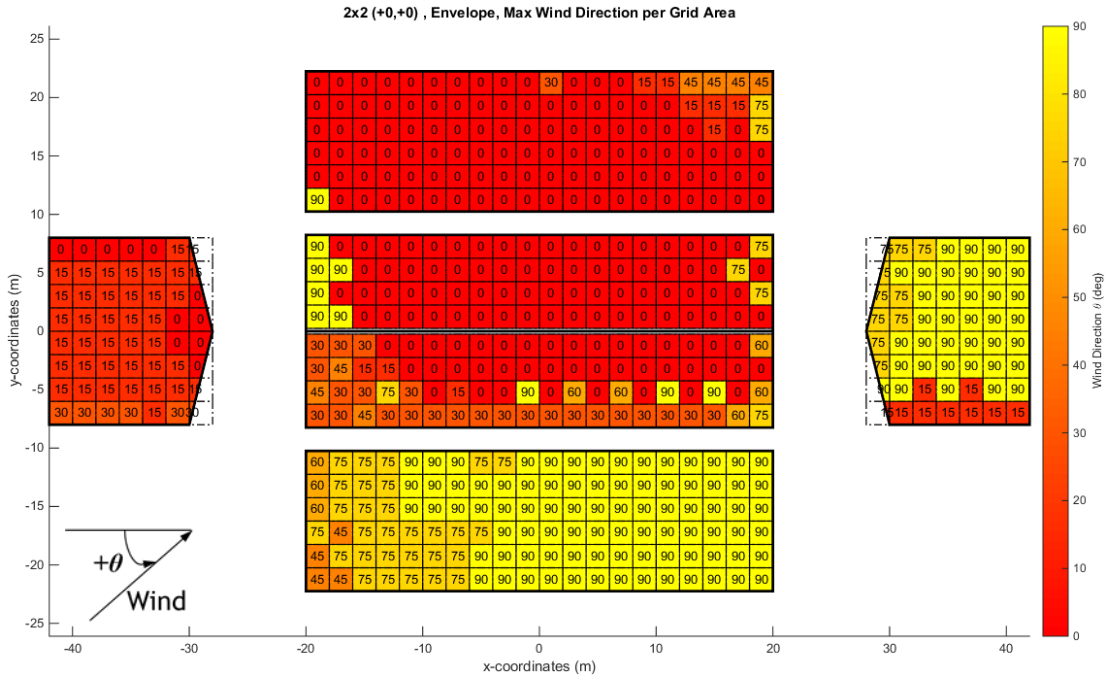

Figure 4.35: Worst case wind angles for the maximum pressures of TPU-3

4.2. Methodology Applied to a Select Building from UWO's Low-Rise Wind Tunnel Database

As the TPU low-rise building without eave wind tunnel database was limited by the pressure tap spacing when observing the effects of wind in the high pressure gradient regions, it became of interest to apply the developed methodology to UWO's wind tunnel database. A building was selected from UWO's database which shared similar dimensions as the previously tested TPU-1 building. The selected gable building has the following dimensions: depth D = 19.05 m (62.5 ft), breadth B = 12.19 m (40 ft), eave height $H0$ = 12.19 m (40 ft), and roof slope of β = 4.76 degrees. The building dimensions are also provided in Table 4.2. To compare with TPU's database which was performed using a suburban terrain exposure category, the exposure category from UWO's database for UWO-1 was selected as suburban terrain.

Table 4.2: Selected building for analysis from UWO's database

Test Label UWO-#	Data Set ID	Roof Type	Breadth B (m)	Depth D (m)	Eave height H0 (m)	Roof Pitch β (degrees)
UWO-1	jp2	Gable	12.19	19.05	12.19	4.76

As can be observed from a flattened plot of the building geometry and pressure tap locations, the distribution of the pressure taps is irregular. Applying the Voronoi diagram provided the tributary areas of the irregularly spaced pressure taps. A plot of the flattened building surfaces, along with the pressure tap locations represented by red circles and the tributary area boundaries represented by blue lines and blue circles, is shown in Figure 4.36.

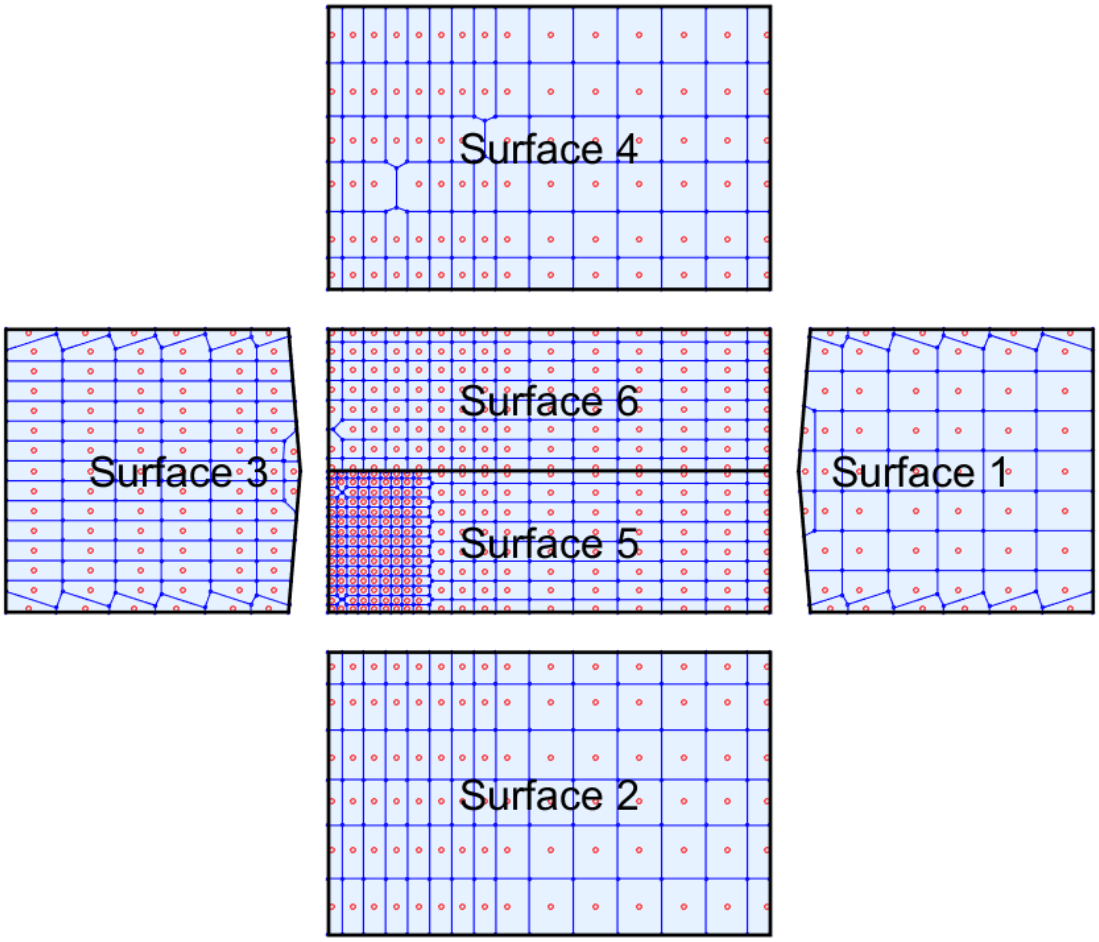

Figure 4.36: Plot of pressure tap locations and tributary areas for UWO-1

The next step for implementing the methodology involves deciding appropriate grid areas. However, as demonstrated in Table 4.3, UWO's database contains much more data for each building than TPU's database with regards to the amount of pressure taps tested, the number of wind directions tested, and the wind tunnel test duration length. Therefore, the time required to perform the analysis on one grid area combination for a relatively small area was very large. For instance, the length of time required to run the grid area combination of 2 ft × 2 ft with no offset in each direction was approximately 24 hours. The peak envelope external pressure coefficient results

are presented for the grid area combination of 2 ft × 2 ft with no offset in each direction, for all 37 wind directions tested, in Figure 4.37 and Figure 4.38.

Table 4.3: Comparison of UWO-1 with TPU-1

Test Label	UWO-1	TPU-1
# of Pressure Taps	688	240
# of Wind Directions	37	7
Full-scale Test Duration (min)	60	10

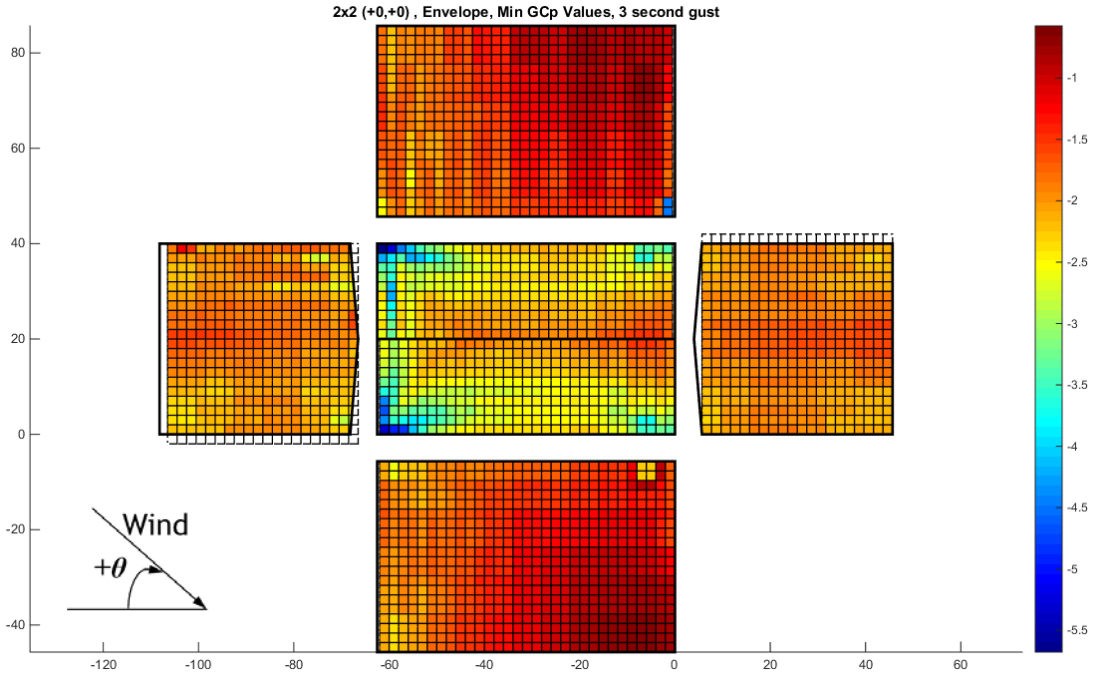

Figure 4.37: UWO-1 Envelope of minimum peak external pressure coefficients for 2 ft × 2 ft grid area (no offset)

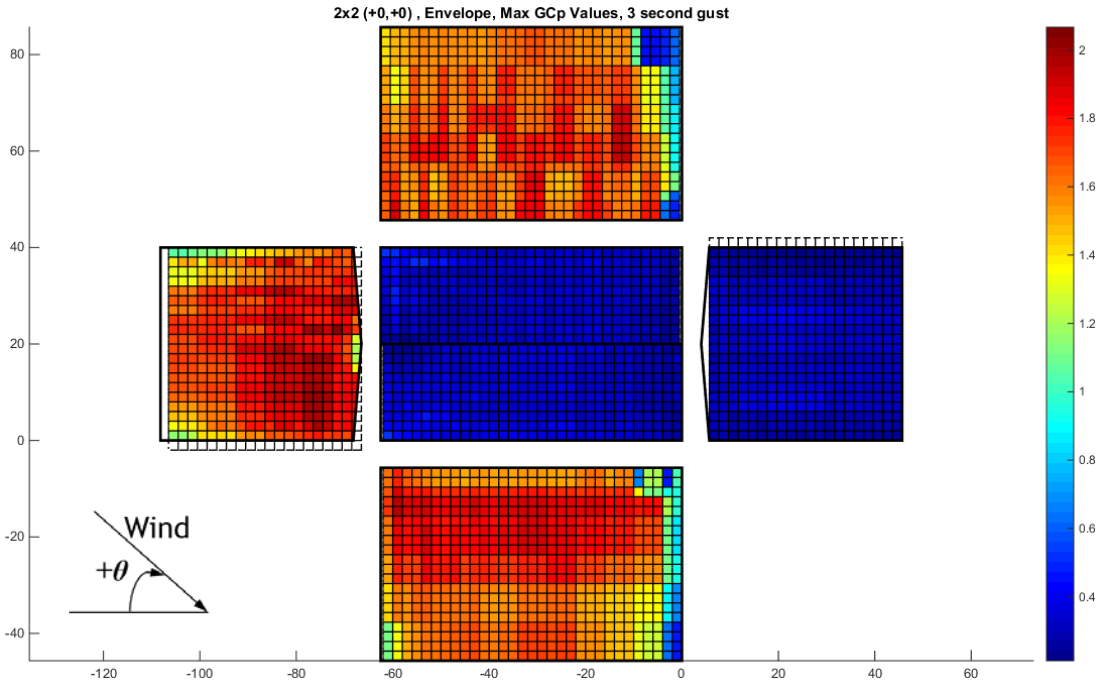

Figure 4.38: UWO-1 Envelope of maximum peak external pressure coefficients for 2 ft × 2 ft grid area (no offset)

4.3. Comparison of TPU-1 and UWO-1 Results for Similar Wind Angles

A comparison was made between TPU-1 and UWO-1 to observe the envelope minimum peak pressure results obtained from both databases, for similar buildings. As TPU's database was limited to seven tested wind angles, seven similar wind angles were selected from UWO's database to produce comparable results. Figure 4.39 represents the envelope of the peak pressure coefficients for TPU-1, where the coordinate system used is in meters. Figure 4.40 represents the envelope of the seven selected wind directions similar to TPU's tested directions for UWO-1, where the coordinate system used is in feet. The external pressure coefficient color scale used is consistent between both figures in that the range is from 0 to -6.

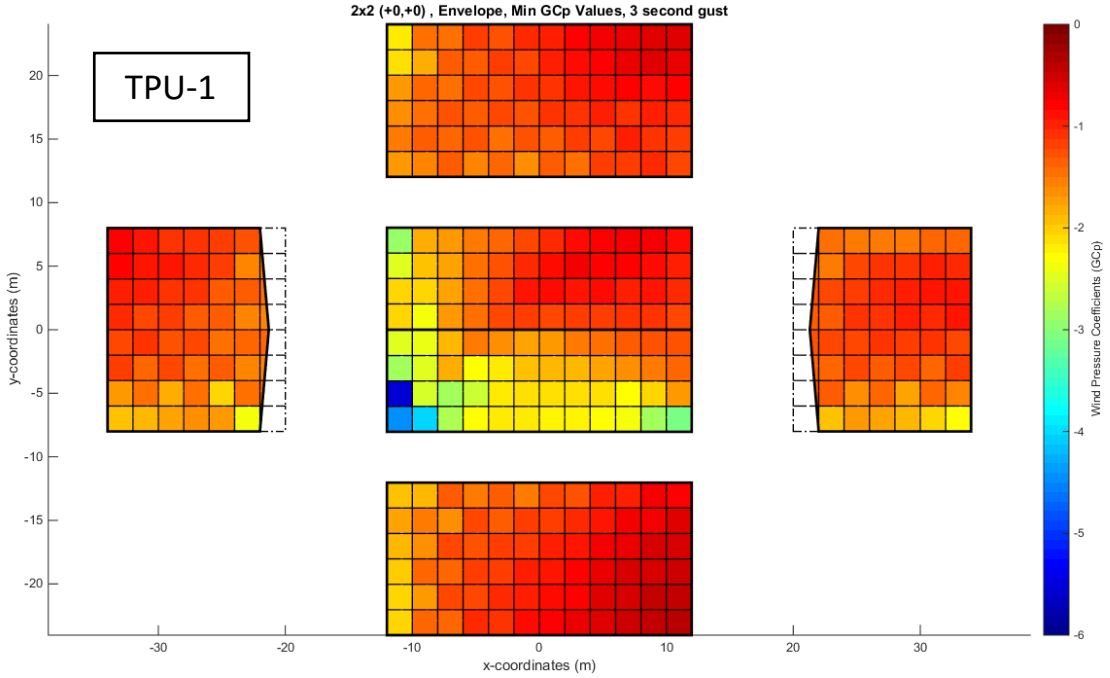

Figure 4.39: Envelope of peak external pressure coefficients for TPU-1

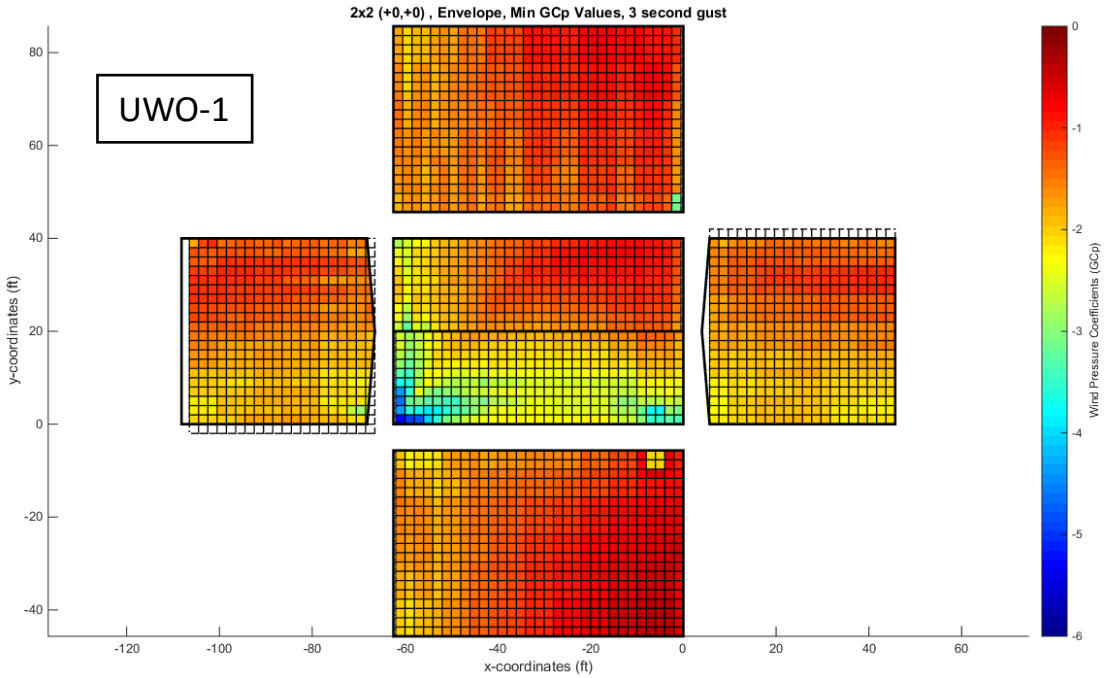

Figure 4.40: Envelope of peak external pressure coefficients for UWO-1

4.4. Discussion

The methodology developed for analyzing the external pressure coefficients from wind tunnel testing data was presented and outlined. The methodology adapted specific features to aid in the computational analysis such as the Voronoi diagram, and the procedure of superposing, incrementing and offsetting grid areas. Applying the developed methodology to TPU's and UWO's low-rise building wind tunnel databases, allowed for the comparison with existing external pressure coefficients defined in ASCE 7-10.

The TPU and UWO low-rise wind tunnel databases each contain a vast amount of data for the analysis of wind loads. However, each of the databases contain their own advantages and disadvantages which are briefly reviewed as follows. The first phase of UWO's wind tunnel database does not contain a large variety of tested geometric plan dimensions such as TPU's database. However, the models that were tested contain a high resolution of pressure taps for areas of large pressure gradients like the windward corner of the gable roof buildings. As TPU's database does not contain a fine resolution of pressure taps in this region, UWO's database has the advantage. On the other hand, TPU's database provides test data for a greater variety of building geometries.

Hagos et. al. (2014) performed a study comparing three similar buildings from the two databases and found that the peak pressure results from the examined pressure taps show minor differences between the two databases, and are therefore regarded as equally valid. As such, the two databases each provide significant value for the purpose of analyzing wind effects on low-rise buildings. The study performed by Hagos et. al. (2014) is similar to this study, but instead of considering only three to five pressure

taps and three wind directions, this developed methodology considers all pressure taps and all wind directions.

In this study, the methodology was applied to three selected buildings from TPU's database TPU-1, TPU-2 and TPU-3, which are listed along with their dimensions in Table 4.1, and were selected to be the same buildings evaluated by Hagos et. al. (2014). Multiple plots were produced to aid in the evaluation of the external pressure coefficients. The first set of figures from the results presented the tributary areas of the pressure taps, which were calculated using the Voronoi diagram and displayed the irregular pressure tap distributions along the surfaces of the building.

The second set of figures presented the peak external pressure coefficients of TPU-1 for all of the tested wind directions. All of the wind directions must be evaluated to produce the envelope of the peak external pressure coefficients that was subsequently presented for a grid area combination of 2 m × 2 m with no offset in the third set of figures. A color bar was provided for the determination of the peak pressure in each respective grid area. Examination of the figures indicates that the worst case suction pressures occur in the windward exterior corner of the roof for the three buildings tested. The figures representing the peak pressure coefficients of TPU-2 and TPU-3 contain an interesting pattern as the layout of the grid include grid areas that become weighted averaged when overlapping with two or more pressure tap tributary areas. For this reason, the offset and incrementing of grid areas becomes valuable and effective in analyzing the worst case peak values to populate the figures which collect the peak pressure coefficient values by their zone. In Figure 4.22 the peak pressure coefficient results from TPU-3 contain what appears to be a thick grey line on the ridge

of the gable roof, this is a result of the roof pitch being slightly greater than the other tested buildings; therefore, when flattening the roof, the roof breadth dimension is slightly larger than TPU-1 and TPU-2.

The fourth set of figures provides the zone layout of each building from which the external pressure coefficients were assigned to their respective zone, based on their grid area size and location. A rule was enforced for partial grid areas where they were considered in a zone if at least 50% of the grid area fell inside of the zone; this partial grid area scheme was applied only for the exterior zones 2, 3 and 5.

The fifth set of figures contains the peak external wind pressure coefficients sorted by their respective zone. These figures include the recommended external pressure coefficients specified by ASCE 7-10 overlaid for visual comparison. A frequent discontinuity in the data for the maximum pressure results, and less frequently for the minimum pressure results, can be observed in some of the figures; this is attributed to the collection of data sets corresponding to different wind directions, as the same surfaces can experience completely different pressures depending on the wind direction. It can be observed via these plots, that the current ASCE 7-10 specifications for the external pressure coefficients on the components and cladding of low-rise buildings are under predicted for all corner, edge, and interior zones of the roof, especially for the negative pressures (suction); similarly, the specifications for the external pressure coefficients on the wall surfaces are under predicted, in both negative (suction) and positive (applied) pressures.

The sixth set of figures was developed to understand which wind direction was causing the worst case minimum or maximum peak envelope pressure in each grid area.

The lack of symmetry in these figures is attributed to the limited amount of wind angles tested, between 0 and 90 degrees, where as if the building was tested between 0 and 360 degrees, the results would contain higher levels of symmetry.

Following the study of the three selected buildings from TPU's database, the application of the methodology was performed on one selected similar building from UWO's database UWO-1, which was listed along with its dimensions in Table 4.2. The first figure presented the tributary areas of the pressure taps, which were calculated using the Voronoi diagram and displayed the irregular pressure tap distributions along the surfaces of the building. However, due to the considerable size of UWO's database in comparison to TPU's database, the developed methodology was only performed on one grid area combination for the sake of time required to perform an entire test. Therefore, the peak envelope external pressure coefficient results were presented for the grid area combination of 2 ft × 2 ft with no offset in the second set of figures. As UWO's database contains many more pressure taps in the corner region of the roof, reducing the size of the grid area provides a better representation of the wind loading effects; as such, the behavior of the suction pressure can be clearly represented through Figure 4.37.

A comparison was then made between the envelope minimum peak pressure coefficients of TPU-1 and UWO-1, considering only similar tested wind angles. The figures obtained from this comparison show similar results between the two tested buildings for the two distinct wind tunnel databases. The worst case external pressure coefficient minimum peak value for TPU-1 over all 2 m × 2 m grid areas was -5.541. While, the worst case external pressure coefficient minimum peak value for UWO-1 over all 2 ft

× 2 ft grid areas was -5.297. The percent difference between the two worst case values of TPU-1 and UWO-1 is therefore 4.61%.

Chapter 5: Conclusion and Future Studies

5.1. Conclusion

This study focuses on a procedure to analyze aerodynamic databases for low-rise structures with the goal of assessing the adequacy of ASCE 7-10 wind provisions for components and cladding. The details of the wind tunnel databases subjected for analysis were summarized. Through the subsequent sections, a methodology for analyzing a wind tunnel database was outlined step by step and explained in a method which can be reproduced to obtain similar results. The Voronoi diagram provided a rational approach to assign the pressure coefficient time history data measured at discrete, irregularly spaced points to areas that contain these points. The proposed method was applied to three buildings from TPU's database and one building from UWO's database. Comparison between the results from the tested TPU buildings and the ASCE 7-10 recommended coefficients showed that the external pressure coefficient recommendations to all zones are under predicted, for the buildings which were tested. Comparison between a similar building from TPU's and UWO's database, for seven similar wind directions, showed that the wind tunnel testing data obtained through each database provides consistent results among the databases. This similarity can be used to reinforce the validity of the developed methodology and also justify the conclusion made by Hagos et. al. (2014) for which the databases can be qualified as equally valid. Based on these results, it was concluded that the current ASCE 7-10 specifications for components and cladding need to be updated.

5.2. Future Studies

It is of interest to expand this research to analyze the collection of low-rise buildings tested in the wind tunnel databases for each of TPU's and UWO's database. This study focused mainly on the methodology developed for evaluating the external pressure coefficients. As the results conclude that the external pressure coefficients for the analysis of components and cladding in the current ASCE 7-10 specifications are under predicted, a future area of interest would be to evaluate many of the database's tested buildings and propose corrections to the current specifications. Such amendments to the specifications could include changes to the zone size/geometry, in order to improve the effectiveness of applying the strongest pressure coefficients to their rightful areas.

Another open area for exploration is evaluating the various options of curve fitting functions for peak estimations. There are currently many available methods for predicting the minimum and maximum peaks of a given time series. As it is important for the fitted curves to accurately match the extreme values and tails of the distribution's histogram, future studies could be done regarding the goodness of fit of such available methods.

References

1. AIJ (Architectural Institute of Japan). (2004). Recommendations for Loads on Buildings, Japan.

2. ASCE/SEI (American Society of Civil Engineers/Structural Engineering Institute). (2010). "Minimum Design Loads for Buildings and Other Structures." *ASCE 7-10*, Reston, VA.

3. Delaunay, B. (1934). "On the Empty Sphere." In Memory of Georges Voronoi, *Bulletin of the USSR Academy of Sciences, Section: Mathematics and Natural Sciences*. 6, 793-800.

4. Durst, C.S. (1960). "Wind Speeds Over Short Periods of Time." *Meteor. Mag.* 89(1056), 181-187.

5. Duthinh, D., Main, J.A., Phillips, B.M. (2015). "Methodology to Analyze Wind Pressure Data on Components and Cladding of Low-Rise Buildings." NIST Technical Note. *National Institute of Standards and Technology*, Gaithersburg, MD.

6. Gavanski, E., Gurley, K.R., Kopp, G.A. (2013). "Uncertainties in the estimation of peak pressures on low-rise building with Gumbel fitting approach." *The 12th Americas Conf. on Wind Eng. (12ACWE)*. Seattle, WA.

7. Hagos, A., Habte, F., Chowdhury, A., and Yeo, D. (2014). "Comparisons of Two Wind Tunnel Pressure Databases and Partial Validation against Full-Scale

Measurements." *J. Struct. Eng.*, 10.1061/(ASCE)ST.1943-541X.0001001, 04014065.

8. Ho, T.C.E., Surry, D., and Morrish, D. (2003). "NIST/TTU cooperative agreement/windstorm mitigation initiative: wind tunnel experiments on generic low buildings." *BLWT-SS20-2003*, Boundary Layer Wind Tunnel Laboratory, Univ. of Western Ontario, London, Canada.

9. Lieblein, J. (1974). "Efficient Methods of Extreme-Value Methodology." *National Bureau of Standards*, Washington D.C. 74, 247-276.

10. Main, J.A. (2011). "Special-Purpose Software: MATLAB Functions for Estimation of Peaks from Time Series." *National Institute of Standards and Technology*, Gaithersburg, MD, ⟨*www.itl.nist.gov/div898/winds/peakest_files/peakest.htm*⟩ (Sept. 29, 2015).

11. MATLAB. (2014). MATLAB documentation 2014b. *The Mathworks, Inc*.

12. NIST (National Institute of Standards and Technology) Statistical Engineering Division. (2004). "Extreme Winds and Wind Effects on Structures." *National Institute of Standards and Technology*, Gaithersburg, MD, ⟨*http://www.itl.nist.gov/div898/winds/homepage.htm*⟩ (Sept. 29, 2015).

13. Peng, X., Yang, L., Gurley, K., Prevatt, D., Gavanski, E. (2013). "Prediction of peak wind loads on a low-rise building." *Proc., 12th Americas Conf. on Wind Eng.*, Seattle, WA.

14. Rice, S.O. (1944). “Mathematical analysis of random noise.” *Select papers on noise and stochastic processes*, N. Wax, ed., Dover, NY.

15. Sadek, F., Simiu, E. (2002). “Peak Non-Gaussian Wind Effects for Database-Assisted Low-Rise Building Design.” *J. Eng. Mech.*, 10.1061/(ASCE)0733-9399(2002), 128(5), 530-539.

16. Sievers, J. (2015). “VoronoiLimit.” *MATLAB Central File Exchange*, ⟨*http://www.mathworks.com/matlabcentral/fileexchange/34428-voronoilimit*⟩ (Apr. 9, 2015).

17. Simiu, E. (2011). *Design of Buildings for Wind: A Guide for ASCE 7-10 Standard User and Designers of Special Structures*. Wiley, Hoboken, NJ.

18. Tamura, Y. (2012). “Aerodynamic Database of Low-rise Buildings.” Global Center of Excellence Program, Tokyo Polytechnic University, Tokyo, Japan, ⟨http://www.wind.arch.t-kougei.ac.jp/info_center/windpressure/lowrise/mainpage.html⟩ (Sept. 29, 2015).

19. Voronoi, G. (1908). “New Applications of Continuous Parameters to the Theory of Quadratic Forms.” *J. of Pure and Applied Mathematics*, 133(133), 97-178. doi:10.1515/crll.1908.133.97.